Journal of Molecular Liquids 422 (2025) 127142

Contents lists available at ScienceDirect

Journal of Molecular Liquids

journal homepage: www.elsevier.com/locate/molliq

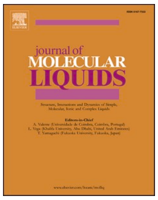

Computational study of eco-friendly PFOA extraction via matrine-based low melting mixture

Sonia Martel-Martín [a], Nuria Aguilar [b], Alberto Gutiérrez [b], Sara Rozas [b], Pedro A. Marcos [c], Alfredo Bol [a,c], Mert Atilhan [d], Jose L. Trenzado [e], Santiago Aparicio [a,b,*]

[a] International Research Centre in Critical Raw Materials-ICCRAM, University of Burgos, 09001 Burgos, Spain
[b] Department of Chemistry, University of Burgos, 09001 Burgos, Spain
[c] Department of Physics, University of Burgos, 09001 Burgos, Spain
[d] Department of Chemical and Paper Engineering, Western Michigan University, Kalamazoo, MI 49008-5462, USA
[e] Department of Physics, University of Las Palmas de Gran Canaria, 35017 Las Palmas, G.C., Spain

ARTICLE INFO

Keywords:
PFAS remediation
Deep eutectic solvents (DES)
Low Melting Mixtures (LMM)
Matrine
Hydrophobic extraction
Environmental contamination
Multiscale theoretical approach

ABSTRACT

Per- and polyfluoroalkyl substances (PFAS) are synthetic chemicals widely used in industrial applications and consumer products for their exceptional stability and resistance to degradation. However, these same properties make PFAS persistent environmental pollutants, posing significant risks to human health and ecosystems. Conventional methods for PFAS removal from contaminated water such as activated carbon adsorption, ion exchange, and advanced oxidation processes, have limitations, including high costs, energy requirements, and incomplete degradation. In response to these challenges, Deep Eutectic Solvents (DESs) and Low Melting Mixtures (LMMs) have emerged as promising alternatives. This study explores the use of matrine-based hydrophobic LMM for the extraction of PFAS from polluted water. Matrine, an alkaloid derived from *Sophora flavescens*, enables the formation of hydrophobic LMM with tunable properties that enhance PFAS extraction efficiency. The unique characteristics of LMM, including biodegradability, low volatility, and selective interaction with PFAS suggest they could provide a more sustainable and effective solution for PFAS remediation. This paper investigates the potential of matrine-based hydrophobic LMM and other similar LMMs with enhanced environmental and toxicological profiles, as well as their additional effectiveness in extracting PFAS from polluted water. The research operates within the Safe an Sustainable by Design (SSbD) paradigm, assessing potential environmental and toxicological issues of the proposed solution. The aim is to contribute to the development of innovative and environmentally friendly approaches for addressing the persistent problem of PFAS contamination in water.

1. Introduction

Per- and polyfluoroalkyl substances (PFAS) are a group of over 7000 synthetic chemicals, known for their unique properties such as water and oil repellence, chemical resistance, and surfactant nature [1]. They are extensively used in various applications: coatings, paints, firefighting foams, and food packaging due to their exceptional stability and persistence, stemming from the strong carbon–fluorine bond [2]. PFAS exhibit high persistence in the environment resulting from their resistance to degradation, leading to long-lasting contamination issues ("*forever chemicals*"), although certain recent studies have showed possible pathways for microbial biodegradation [3]. PFAS pose a significant challenge as they persist in groundwater even decades after their initial use, exceeding regulatory limits by significant margins [4]. The extreme persistence of PFAS, characterized by their resistance to environmental and metabolic degradation, classifies them under the Persistent Organic Pollutant (POPs) European regulations [5], necessitating a phased approach to eliminate non-essential uses to prevent escalating concentrations and associated adverse effects. The high mobility of PFAS in soil and groundwater, coupled with the challenges in purification and treatment processes, further underscores the technical complexity and costliness of reversing PFAS contamination once it occurs. Therefore, PFAS are highly mobile, bio-accumulative, and potentially toxic.

---

* Corresponding author at: International Research Centre in Critical Raw Materials-ICCRAM, University of Burgos, 09001 Burgos, Spain.
E-mail address: sapar@ubu.es (S. Aparicio).

https://doi.org/10.1016/j.molliq.2025.127142
Received 20 December 2024; Received in revised form 6 February 2025; Accepted 10 February 2025

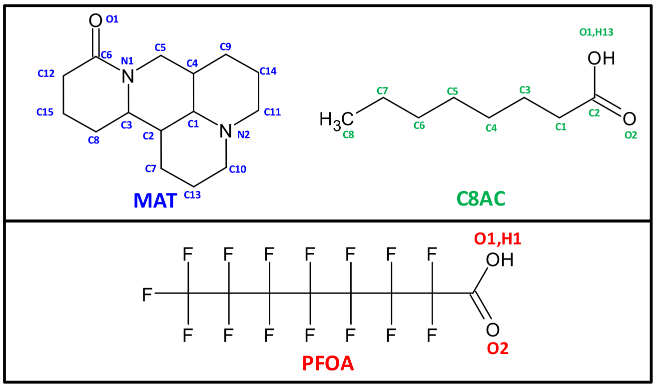

Fig. 1. Molecular structures of compounds used in this work for the developed LMM as well as for PFAS (PFOA).

Regarding environmental PFAS effects, they may contaminate water as PFAS can easily enter water supplies through spills, improper disposal, or even from firefighting foams. They can travel long distances in water and contaminate drinking water sources like lakes, rivers, and groundwater [6]. For the impact on wildlife, animals exposed to PFAS through contaminated water or food can experience various health problems. Studies have shown effects on wildlife immunity, reproduction, and development [7]. Regarding the effects of PFAS on human health, changes in blood chemistry (increased cholesterol and altered liver enzyme levels following PFAS exposure), reduced birth weight (decrease in birth weight for babies born to mothers with higher PFAS levels), or weakened immune system (lowered antibody response to certain vaccines, affecting immune function) have been confirmed [8]. Additional potential effects under study are certain cancers (possible link between PFAS exposure and an increased risk of kidney and testicular cancers), pregnancy complications (induced hypertension and preeclampsia), and other health problems such as altered metabolism and weight regulation, increased risk of type 2 diabetes or thyroid issues, among many others. Therefore, PFAS constitute a long-term environmental and health threat because of their slow degradation and low degradability, allowing them to accumulate in the environment for decades or even centuries.

In the case of PFAS in water [9], regulatory agencies in various countries have established guidelines and limits for PFAS in drinking water. For example, the United States Environmental Protection Agency (EPA) has recently issued health advisories for two common PFAS compounds, PFOA (per-flurooctanoic acid) and PFOS (Perfluorooctane sulfonic acid), setting a combined limit of 4.0 ng/L in drinking water [10]. In the case of EU, these substances are listed under REACH Annex XVII entry 68, e.g. with PFOA limits below 25 ppb [11]. Therefore, PFAS removal from drinking water is a requirement according to the increasingly strict world laws.

Various technologies have been developed to remove PFAS from contaminated water, including activated carbon adsorption, ion exchange, membrane filtration, and advanced oxidation processes [12,13]. Activated carbon adsorption is one of the most commonly used methods due to its effectiveness in removing a broad range of PFAS, particularly long-chain compounds [14]. However, this method has limitations, such as the reduced efficacy for short-chain PFAS, high operational costs [15], and the need for frequent regeneration or disposal of saturated carbon materials, as well as the current regulations leading to large requirements in PFAS removal, thus increasing operational costs [16]. Ion exchange resins offer another solution by replacing PFAS anions with less harmful ions [17]. While effective, this method also faces challenges, like resin fouling and the high cost of resin regeneration, encountering difficulties for PFAS removal once captured as a result of the large resin-PFAS affinities, or replacement [18]. Membrane filtration techniques [19], such as nanofiltration [20] and reverse osmosis [21] can effectively remove PFAS but are energy-intensive and produce concentrated waste streams that require further treatment [22]. Advanced oxidation processes, including photocatalysis [23], ozonation [24], and electrochemical oxidation [25] aim to degrade PFAS into less harmful byproducts. However, these processes often require high energy inputs, specialized equipment and can produce incomplete degradation, resulting in the formation of potentially harmful intermediates [26].

Given the limitations and problems of conventional PFAS remediation methods, a growing interest in exploring alternative approaches has sprung. Deep Eutectic Solvents (DESs) have emerged as a promising class of solvents for various applications as a result of their tunable properties, low toxicity and environmental compatibility [27]. DESs are formed by mixing two or more components, typically a Hydrogen Bond Donor (HBD) and a hHydrogen Bond Acceptor (HBA), which interact to form a eutectic mixture with a melting point significantly lower than that of the individual components.

A particularly useful type of DESs are the Natural DESs (NADESs) [28], which are formed by combining two or more natural componentslike organic acids, sugars, alcohols, amines, and amino acids through simple mixing. NADESs offer several advantages over traditional organic solvents such as biodegradability, negligible toxicity [29], tunable properties and simple preparation, which make them suitable for several applications including extraction technologies [30]. The removal of PFAS from polluted water through solvent extraction requires that the solvent itself does not contaminate the water, making Hydrophobic NADESs (HNADESs) a suitable option [31]. HNADESs have been designed and successfully applied for the extraction of very different types of hydrophobic compounds including lipids, natural oils and fragrances from plants and other sources [32], as well as for the solubilization of poorly water-soluble drugs [33]. Additionally, HNADESs have been proved for the successful removal of pollutants from water and wastewater [34], including PFAS removal [35]. The use of HNADESs have the double advantage of avoiding water cross-contamination while mantaining their high affinity (task-specific solvents) towardds (hydrophobic) PFAS.

The literature shows a diversity of possible HNADESs, involving molecules such as fatty acids or terpenoids [36]. Recently, a new type of HNADESs based in the natural compound matrine (MAT, Fig. 1) combined with the fatty acid (octanoic acid, C8AC) has been proposed for solubilization of low solubility drugs [37,38]. MAT is a natural alkaloid that can be extracted from plants like *Sophora flavescens* possessing unique chemical properties that make it suitable for forming hydrophobic DESs. Therefore, MAT-based (considering fatty acids) HNADESs are proposed in this work as a proof of concept of task-specific natural solvents to selectively interact with PFAS molecules, enhancing their extraction efficiency from aqueous environments, presenting an alternative technology for PFAS removal from drinking and wastewater.

Nevertheless, from a thermodynamic viewpoint, the DESs definition will strictly rely in the comparison of deviations of experimental Solid-Liquid equilibria curves with ideal ones [39], and thus to address this, some authors [40] have proposed using the term Low Melting Mixtures (LMMs). Therefore, it is pondered that the term (hydrophobic) LMM for the considered MAT:C8AC system is more suitable and therefore, will be used along this work.

The archetypical perfluorooctanoic acid (PFOA) has been considered as a representative of PFAS as it is found to be among the most abundant PFAS in water and wastewater [41],

A multiscale theoretical approach is designed and applied to study the solubilization and extraction from water of MAT:C8AC (1:1) LMM. The objectives of this study are: *i*) understanding LMM properties with particular attention to intermolecular forces (hydrogen bonding), *ii*) analyzing the nanoscopic mechanism(s) of PFAS extraction using PFOA as PFAS model, *iii*) confirming the suitability of the considered LMM for PFAS removal for drinking water, and *iv*) proposing a new LMM with enhanced environmental and toxicological profiles and extra extractive

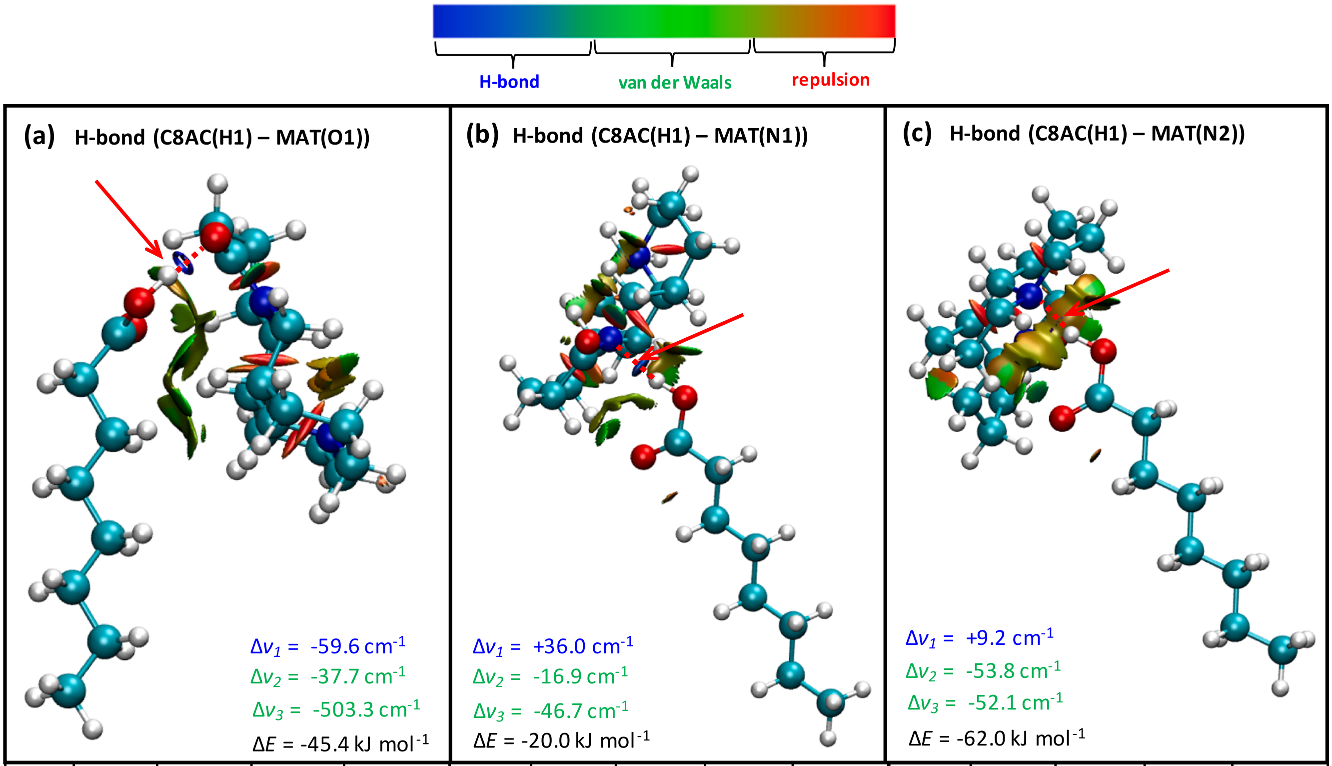

r / Å	α / deg	ρ_e / a.u.	$\nabla^2\rho_e$ / a.u.	CVB / a.u.	r / Å	α / deg	ρ_e / a.u.	$\nabla^2\rho_e$ / a.u.	CVB / a.u.	r / Å	α / deg	ρ_e / a.u.	$\nabla^2\rho_e$ / a.u.	CVB / a.u.
1.62	174.5	0.0555	0.1212	-0.1125	1.89	169.2	0.0368	0.0737	-0.0918	1.63	162.8	0.0682	0.1258	-0.2657

Fig. 2. DFT optimized structures of MAT:C8AC–dimer for three different hydrogen bonding structures. Interaction energy, Δ*E*; Hydrogen bonding distance (*r*) and angle (α); QTAIM properties (ρ_e and $\nabla^2\rho_e$), Core Valence Bifurcation index (CVB) for the relevant hydrogen bonds; NCI analysis and (red) shifting of relevant vibration stretching frequencies $\Delta\nu_1$ (C═O in MAT stretching), $\Delta\nu_2$ (C═O in C8AC stretching) and $\Delta\nu_3$ (O—H in C8AC stretching) upon cluster formation.

effectiveness. The use of MAT:C8AC is a more sustainable and effective alternative to conventional remediation technologies. Additionally, molecular modifications of the LMM components were designed using Machine Learning (ML) to improve characteristics of the designed LMM solvent to allow its scalability for water processing purposes.

2. Materials and methods

2.1. Quantum chemistry calculations

Density Functional Theory (DFT) calculations were employed to analyze the hydrogen bonding interactions between molecules in the system. Specifically, the BP86/def2-TZVP level of theory with Grimme's D3 [42] correction was used within the Turbomole software package [43]. This approach allowed to investigate the formation and strength of hydrogen bonds in clusters containing MAT-C8AC molecules, with and without the presence of PFOA. To quantify the interaction strength, the binding energy for each cluster (Δ*E*) was calculated as the difference between the cluster's total energy and the sum of the individual molecules energies. A correction factor was applied to account for a potential Basis Set Superposition Error (BSSE) [44]. Furthermore, a topological analysis of the intermolecular interactions was carried out using Bader's Quantum Theory of Atoms in Molecules (QTAIM [45]) with the help of MultiWFN software [46]. This analysis involved examining various properties like electron density (ρ_e) and Laplacian of electron density ($\nabla^2\rho_e$). Additionally, the Core-Valence Bifurcation Index (CVB [47]) and Non-Covalent Interaction (NCI [48]) analyses were conducted. By investigating these properties, a deeper understanding of the nature and characteristics of the hydrogen bonds formed between the molecules within the clusters was gained.

2.2. COSMO calculations

COSMOtherm calculations were performed using the optimized DFT structures and COSMOthermX software [49]. The corresponding *cosmo* files were generated at the BP86/def-TZVP level to predict the properties of the studied LMM. These calculations within COSMO relied on the individual *cosmo* files for the isolated HBA (Hydrogen Bond Acceptor) and HBD (Hydrogen Bond Donor) molecules within the LMM, as well as for PFOA.

Additionally, the considered LMM was studied interacting with a model lipid bilayer formed by DPPC lipid molecules using the COSMOperm method [50]. This lipid bilayer may be considered as model of a plasma cell membrane and thus it may be established as model of the interaction of the considered molecules and cells, thus allowing to infer possible toxic effects of the materials, as it may be considered as a Molecular Initiating Event (MIE) of the Adverse Outcome Pathway (AOP) for the toxicity of nanomaterials [51,52,53].

2.3. Molecular dynamics simulations

Classical Molecular Dynamics (MD) simulations were carried out with the Forcite module within Biovia Materials Studio software [48]. MD simulations were performed using the COMPASS III force field within Biovia Materials Studio software. Temperature control was done with the Nose-Hoover thermostat and pressure was controlled with the

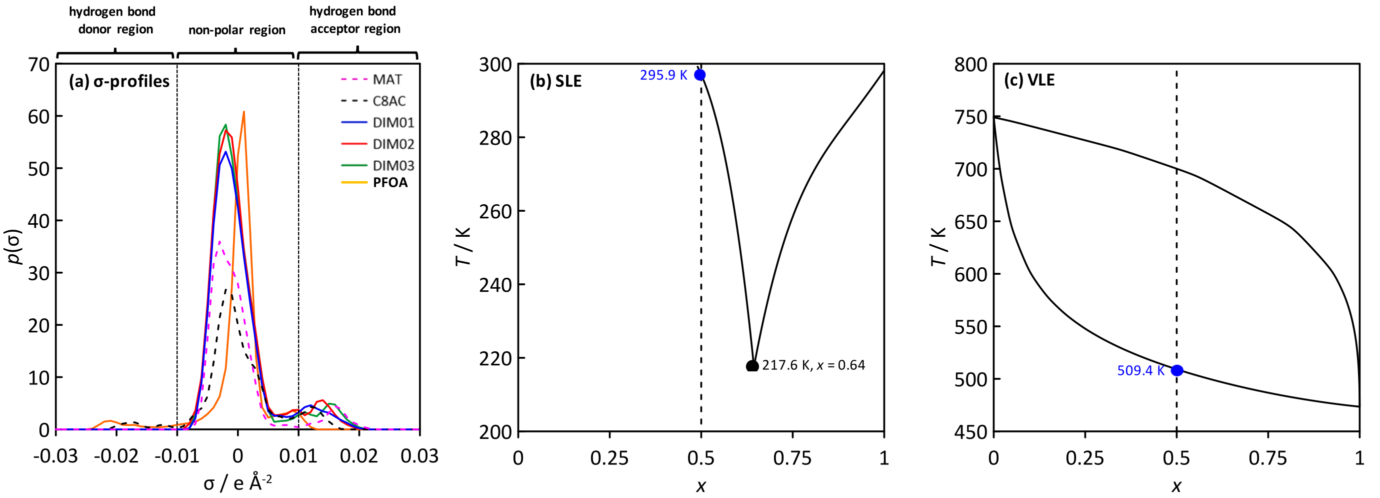

Fig. 3. (a) COSMOtherm σ-profiles, and isobaric ($p = 1$ bar) (a) solid–liquid and (b) vapor–liquid equilibria for x C8AC + $(1 - x)$ MAT calculated with COSMOtherm. Blue dots indicate (a) melting and (b) boiling points of equimolar MAT:C8AC:system (LMM used along this work). Black dot in panel a indicates eutectic composition and temperature.

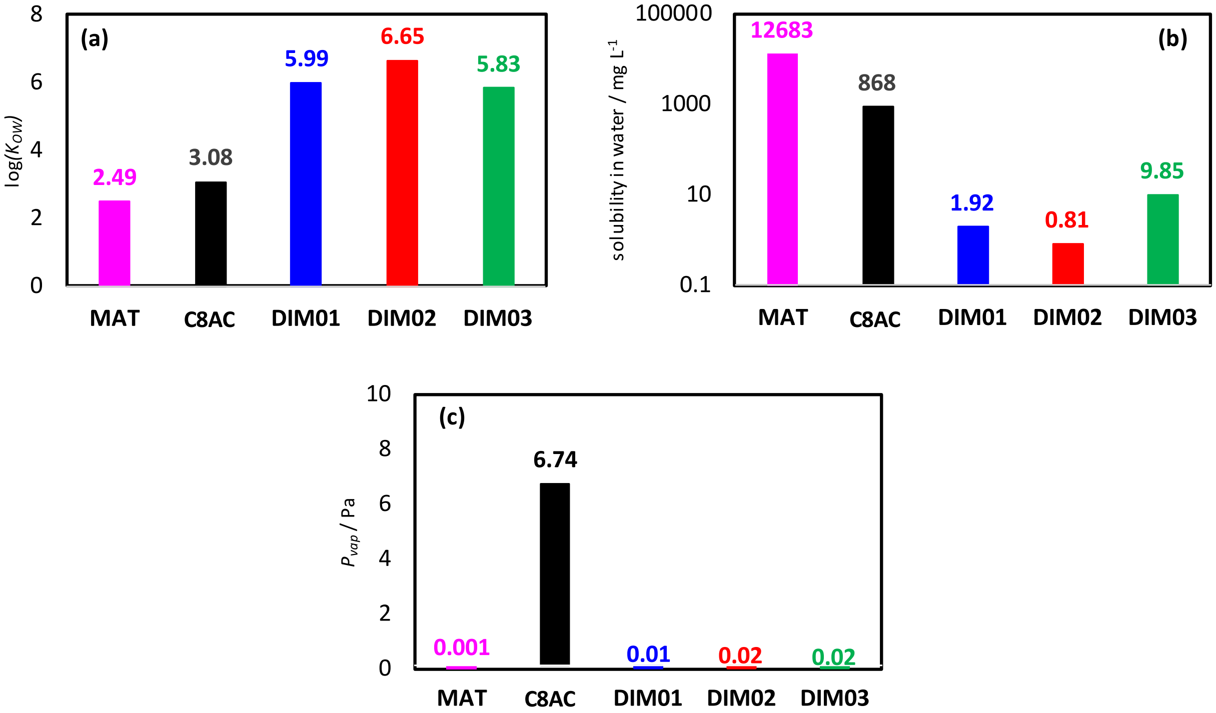

Fig. 4. Results from COSMOtherm for environmentally relevant properties for the considered LMM. (a) octanol–water partition coefficient, K_{OW}; (b) LMM solubility in water; (c) vapor pressure, P_{vap}. All values calculated at 298.15 K.

Parrinello–Rahman barostat. Long-range electrostatics were handled with the Ewald summation method and van der Waals interactions used the Waldman–Hagler mixing rule with a cutoff of 15 Å. Two types of MD simulations were carried out: *i*) pure MAT:C8AC (1:1) LMM, for which cubic simulation boxes containing 500 molecules of each type were built with simulations in the NPT ensemble at 1 bar at temperatures of 298, 308, 318 and 328 K were carried out, and *ii*) simulations of biphasic systems composed by MAT:C8AC (1:1) LMM in contact with a water liquid phase containing 5 wt% PFOA, for which simulations in the NPT ensemble at 1 bar and 328 K were carried out. Data analysis for all MD results, involving visualization and processing, were carried out with VMD and TRAVIS software.

2.4. Screening of molecular diversity around MAT molecular moiety

Considering MAT as a platform molecule for developing LMMs combined with fatty acids, similar molecules to MAT where selected from Zinc Database [54] considering Tanimoto criteria of similarity, from which those 100 on the top were selected (Supplementary Information, screening_results.xlsx). The structures of these molecules were optimized as described in Section 2.1 and *cosmo* files obtained as in Section 2.2. Eutectic composition for all the considered combinations were predicted, as well as PFOA solubility, from COSMOtherm method. To consider the safety and environmental aspects of the possible alternative systems (Safe and Sustainable by Design, SSbD, approach), (toxicity) descriptors considering these components were calculated

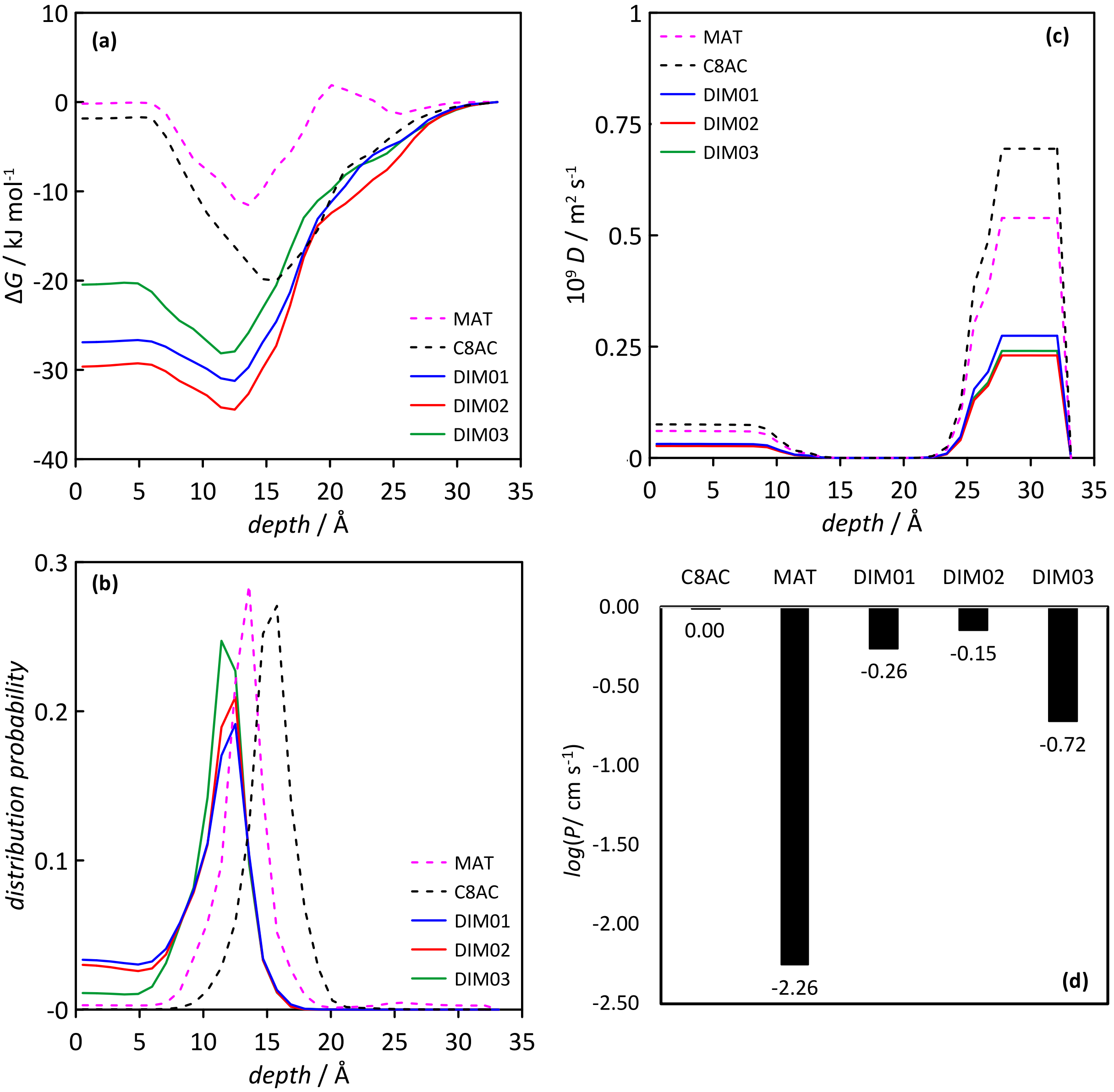

Fig. 5. COSMOperm results for the interaction between the reported systems and DPPC lipid bilayer: (a) free energy profiles, Δ*G*, (b) distribution probability, (c) self-diffusion coefficient through bilayer, *D*, and (d) permeability, *P*. All values calculated at 310.15 K.

from Online Chemical Database [55] as well as suitable environmental properties such as vapor pressure (to quantify possible environmental pollution) and water solubility (to quantify possible water pollution). To infer the most suitable molecule among the 100 obtained, a global score was assigned for each candidate considering melting properties of the possible LMM, PFOA solubility, environmental properties (vapor pressure and water solubility) and toxicological indicators. Likewise, the synthetic ability for the considered molecules was calculated using RDKit [56]. The obtained score led to the most suitable molecule dereived from MAT for LMM development in combination with fatty acids.

3. Results and discussion

3.1. Properties of MAT:C8AC (1:1) LMM

3.1.1. Structural properties: MAT:C8AC (1:1) LMM formation

The properties of the MAT:C8AC LMM are analyze from both structural and dynamic viewpoints to assess its suitability for PFOA absorption. As the considered solvent is a DES, hydrogen bonding develops a pivotal role in its properties and behavior [57]. Thus the nature of the hydrogen bond is studied by means of DFT calculations. MAT molecule is a pure HBA acceptor via three possible sites: an O atom in keto group (O1) and the two N atoms in the corresponding rings (N1 and N2), Fig. 1. Therefore, three possible hydrogen bonds may be established among C8AC (acting as HBD via its OH acidic group) and MAT molecule, Fig. 2a. These three H-bonds lead to large and negative bonding energy Δ*E*, i.e. strong hydrogen bonding is possible through the three MAT sites, but the strength is remarkably different following the ordering N2 > O1 > N1. This may be justified by the fact that the N1 position in MAT is in the vicinity of a CO group, being slightly hindered for the approach of the C8AC molecule. This results in a larger HBA–HBD distance (1.89 Å) in comparison with those via O1 or N2 (1.62 and 1.63 Å, respectively), and thus leading to a weaker interaction. From the viewpoint of QTAIM analysis, the MAT–C8AC hydrogen bonds are characterized by a bond path among the corresponding donor (C8AC) and acceptor (MAT) sites, where a Bond Critical Point (BPC, type (3,−1) according to Bader's terminology [44]) is developed, being characterized by ρ_e and $\nabla^2\rho_e$, Fig. 2. According to Popelier's criteria [58], hydrogen bonds lead to

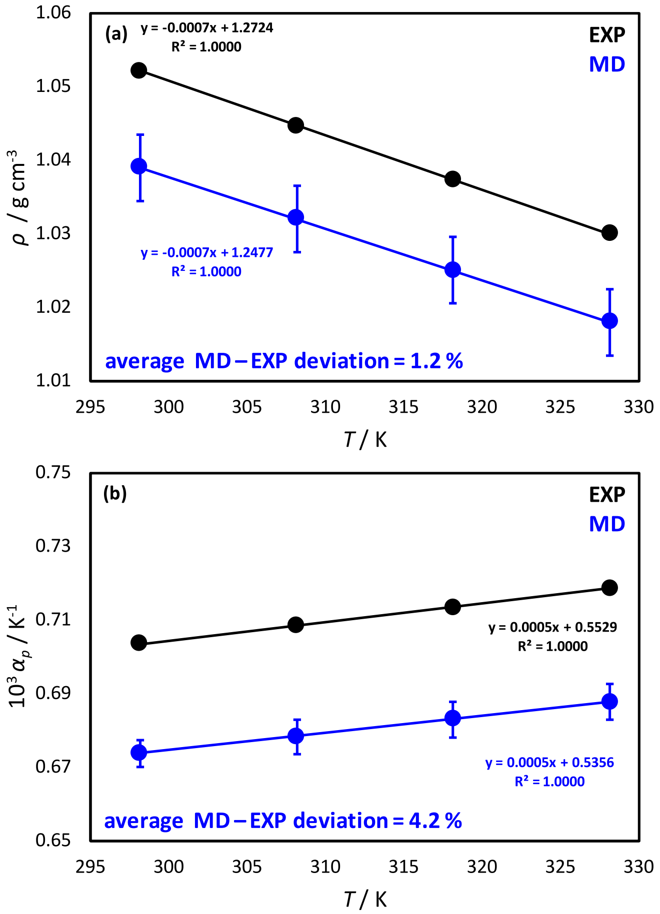

Fig. 6. Comparison among experimental and MD predicted density, ρ, and isobaric thermal expansion coefficient, α_p, for MAT:C8AC(1:1) LMM as a function of temperature. Literature data [39]. Results for linear fits of each property as well as absolute percentage deviations between experimental and MD predicted data are reported inside each panel.

BCPs with ρ_e and $\nabla^2\rho_e$ in the 0.002–0.04 a.u. and 0.020–0.139 a.u ranges respectively, with higher values corresponding to stronger H-bonding. The values for the MAT–C8AC hydrogen bonds are above (for ρ_e) or between this ranges (for $\nabla^2\rho_e$) for the interactions through O1 and N2 MAT sites (larger for N2). In he case of the interaction through N1 is in the middle of these ranges, which justifies the reported ΔE and the strength of the hydrogen bonds. This is also in agreement with the large negative CVB values. NCI analysis shows that all the pairs are characterized by a well localized (blue) spot, ring-shaped closer to the C8AC (OH) group, which characterizes the strong hydrogen bond. Additionally, there is a large region of van der Waals like interactions, more extensive for interactions through the MAT O1 and N2 sites, which would also led to the larger ΔE values. Therefore, the interacting pairs are characterized by very strong hydrogen bonds but also by van der Waals interactions among the hydrophobic moieties of both MAT and C8AC molecules. Likewise, the formation of the hydrogen bond leads to changes in the vibrational properties of the involved bonds. This effect was quantified via the predicted IR spectra for the corresponding pairs (Fig. 2) and its comparison with those of the isolated monomers. The stretching frequency of the MAT(CO) bond suffers remarkable changes upon hydrogen σ-σ-bonding formation, showing red-shifting, which contrasts with the blue shifting for the interaction among the MAT(N) sites and the C8AC(OH) group. The strength of the developed MAT–C8AC interaction is also showed by the large red-shifting of the C8AC(OH) stretching when interacting with MAT(CO) group, whereas this shifting is remarkably lower when interacting via MAT(N) sites. The large red-shifting of C8AC(OH) accompanied by lower redshifting in MAT(CO) are characteristics of hydrogen bonding between acid and keto groups [59]. In contrast, the lower shifting inferred for the interaction via the MAT(N) sites, in spite of the large ΔE, stand from the steric hindrance rising from the situation of N atoms at a shared vortex of two rings.

The optimized structures of the considered monomers (MAT and C8AC), as well as for the corresponding dimers, permit to develop COSMOtherm analysis. This process, starting from the reported σ-profiles, allows to infer donor, acceptor and non-polar regions on the corresponding molecular surfaces, Fig. 3a. These results allow to infer large apolar regions upon dimers formation (intense peaks), which agrees with the NCI results for van der Waals interactions, as reported in Fig. 2. Likewise, the hydrogen bond donor regions vanish upon the dimmer formation while acceptor regions remains. This disappearance of donor regions (because of OH groups from C8AC surrounded by apolar regions, Fig. 2) indicates the prevailing formation of MAT–C8AC dimers in the liquid structuring accompanied by van der Waals interactions among neighbor dimers.

3.1.2. *Thermophysical properties of MAT:C8AC (1:1) LMM: Potential environmental safe use considerations*

The COSMOtherm calculations allowed to infer thermophysical properties of the studied MAT–C8AC LMM, starting from the corresponding isobaric (1 bar) solid–liquid phase equilibria (SLE), Fig. 3b. Although previous literature experimental studies [38,39] proved liquid MAT–C8AC mixtures for several mole ratios, including equimolar ones, the whole SLE, as well as the eutectic composition, had not been reported. The COSMOtherm calculated eutectic point corresponds to roughly 1 MAT: 2 C8AC mixtures with low eutectic temperature, whereas the equimolar mixture shows predicted melting point close to ambient temperature. Therefore, results in Fig. 3b exhibit a wide range of MAT–C8AC mixtures being liquid at ambient temperatures, which can be designed according to the desired hydrophobic nature, increasing C8AC or MAT content, with the considered equimolar mixtures presenting a balance of properties. It should be remarked that the suitability of COSMO method for type V DES/LMM has been probed in the literature even using a single conformer for defining molecular models [60]. In the same way, the isobaric (1 bar) vapor–liquid equilibria (VLE) was predicted, displaying very large normal boiling point for the equimolar mixture, thus negligible evaporation and ultimately, not being a volatile solvent avoiding atmospheric pollution.

Additional possible environmental effects of the potential use of the considered MAT:C8ACLMM are analyzed through properties calculated with COSMOtherm and reported in Fig. 4. The octanol–water partition coefficient, log(K_{OW}), shows low values for the isolated components of the LMM (slightly larger for C8AC than for MAT), but for both molecules these values indicating a large hydrophobic character, Fig. 4a. Upon the formation of MAT:C8AC pairs via hydrogen bonding, in the three considered configurations (Fig. 2a), a synergistic effect is inferred for the calculated log(K_{OW}), reporting very large values, thus showing how the considered LMM is a largely hydrophobic solvent. This effect is also quantified considering the predicted solubility in water, which, although is low for MAT and C8AC (larger for MAT than for C8AC), leads to smaller values upon dimers formation. The large hydrophobic character in the considered molecular pairs rises from the non-polar regions as reported in Fig. 3a. Therefore, these results indicate that when using MAT:C8AC LMM for extracting PFOA from water solutions, no cross contamination will be produced and the presence of the LMM in the aqueous phase will be negligible, considering its extremely low water solubility (Fig. 4b). This low water solubility combined with the negligible calculated vapor pressure (Fig. 4c) indicates that MAT:C8AC LMM is an environmentally friendly solvent, without aqueous or atmospheric emissions, which can be safely used for water treatment operation(s).

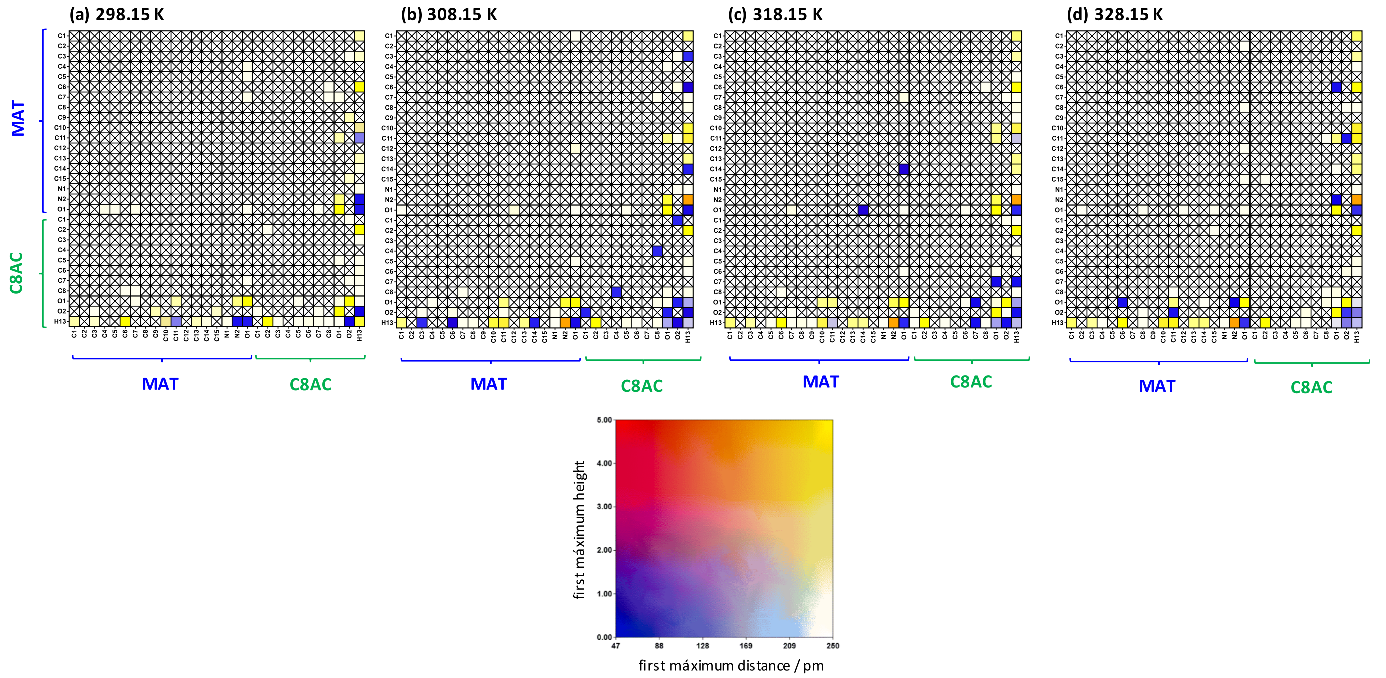

Fig. 7. Connection matrix analysis (cmat) for MAT:C8AC (1:1) LMM mixtures as a function of temperature. Rows and columns show relevant atoms. Atom labelling as in Fig. 1. The color of each square corresponds to the intensity and distance of the first maximum in the corresponding radial distribution functions with the color scale indicated in the panel on the bottom. Atom labelling as in Fig. 1.

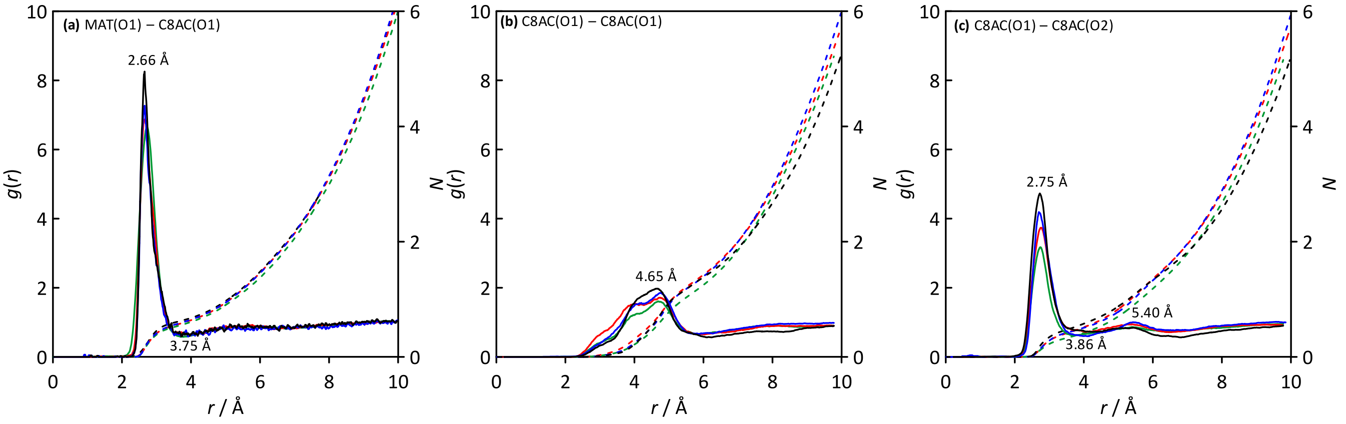

Fig. 8. Site–site Radial Distribution Functions, g(r), for relevant hydrogen bonding sites, and the corresponding integrals, N, for MAT:C8AC (1:1) LMM mixtures as a function of temperature. Atom labelling as in Fig. 1.

3.1.3. Interaction properties of MAT:C8AC (1:1) LMM with model eucariotic wall cells: Potential toxicologicaly safe use considerations

The second issue that must be addressed for the use of MAT:C8AC LMM, once its suitable environmental properties are confirmed, is their possible toxicological effects. It has been proposed in literature to study the interaction of relevant molecules with model lipid membranes to infer their possible cytotoxic effects along with the molecular roots of these interactions and disruptions. This approach has being applied to compounds such as Ionic Liquids [61], which are closely related to the LMM studied in this work. A DPPC lipid bilayer was built and solvated with water molecules as a simplified model of plasma membranes. The interaction of isolated molecules (MAT and C8AC) as well as for MAT; C8AC molecular pairs, in the three considered configurations, with the model membrane was studied using COSMOperm approach [49]. The DPPC lipid molecule has an amphiphilic character, and so the corresponding bilayer, with a polar head (phosphatidylcholine group) and two hydrophobic chains (C16 palmitic acid). Therefore, results in Figs. 3a, 4a and b (very low solubility in water), showing hydrophobic character for all the considered entities, would point to a large affinity for the inner apolar regions of the DPPC model lipid bilayer. Results in Fig. 5a shows the free energy (ΔG) profiles across the membranes for all the molecular entities. The ΔG indicates largely favored penetration in the bilayer, which is improved upon the formation of the MAT:C8AC pairs when comparing with isolated MAT and C8AC molecules, with pairs largely stabilized in the apolar region of the bilayer. These ΔGs do not show any barrier, thus penetration is produced for all the considered cases as a consequence of the largely hydrophobic character (Fig. 4a). Therefore, the MAT:C8AC pairs show maxima of probability for their distribution in the central region of the bilayer. Furthermore, the formation of the pairs allows the penetration into deeper regions of the lipid bilayer in comparison with isolated molecules, Fig. 5b. The diffusion coefficient of the considered molecules across the membrane (Fig. 5c) indicates a rate barrier in the vicinity of the head group (hindered kinetic penetration) but once the polar region is crossed the

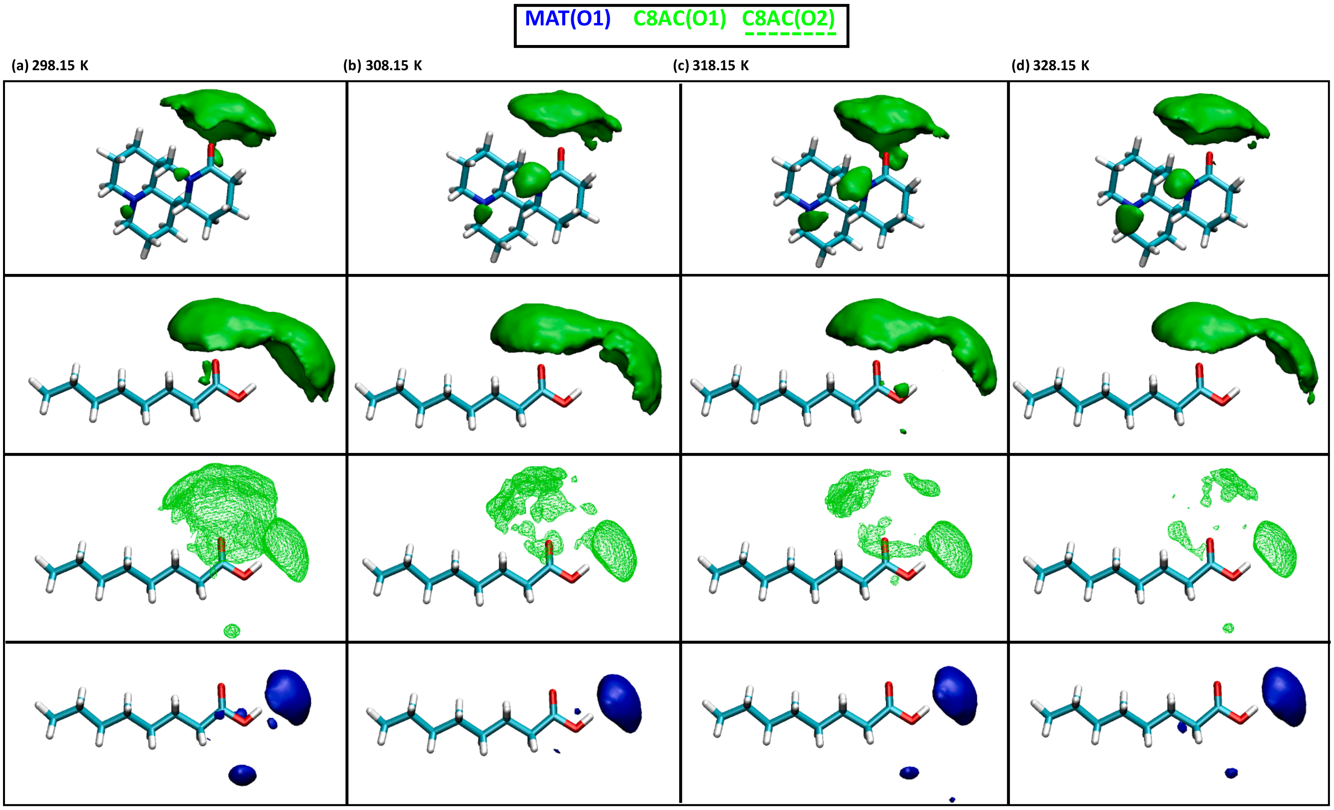

Fig. 9. Spatial Distribution Functions (SDFs) around MAT and C8AC molecules for relevant hydrogen bonding sites, for MAT:C8AC (1:1) LMM mixtures as a function of temperature. Atom labelling as in Fig. 1.

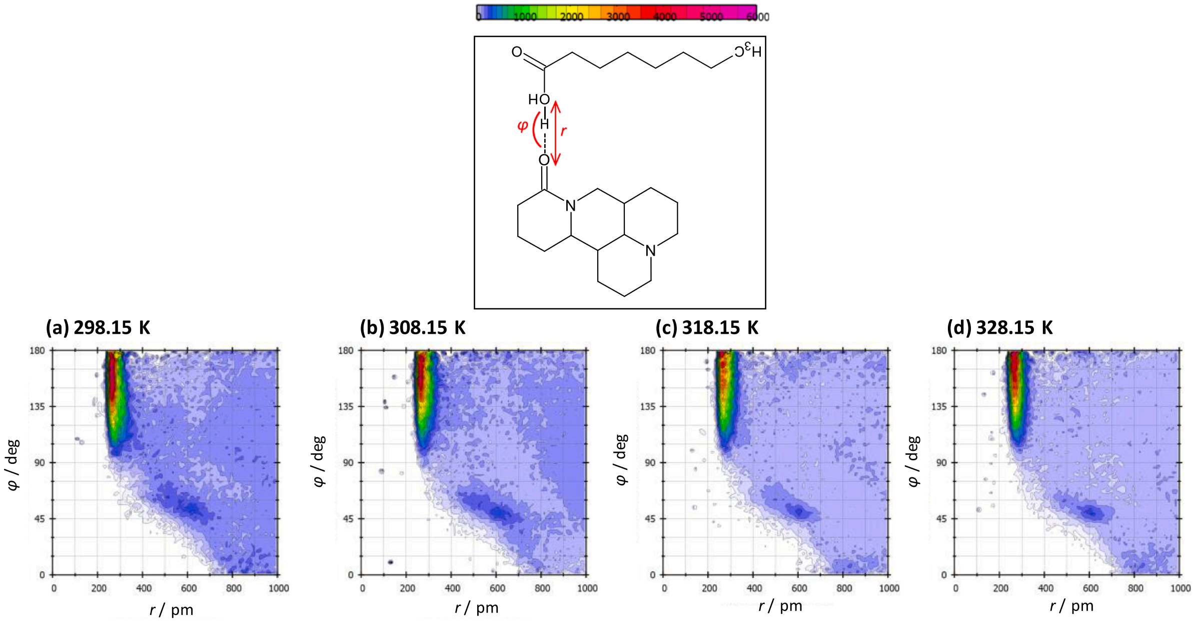

Fig. 10. Combined Distribution Functions (CDFs) for the reported distance, r, and angle, φ, for relevant hydrogen bonding sites, for MAT:C8AC (1:1) LMM mixtures as a function of temperature.

molecules show fast diffusion in the central apolar region of the membrane. It is remarkable that the kinetic barrier decreases upon the formation of MAT:C8AC pairs, in spite of the increase in their hydrophobic character, which may be justified considering steric effects (larger molecular clusters upon pairs formation), leading to disruptive effects on the polar regions of the bilayer, then allowing a faster penetration. Nevertheless, the calculated permeabilities (Fig. 5d) indicate that the considered MAT:C8AC are able to penetrate the lipid bilayer from a kinetic viewpoint, which combined with the favored thermodynamic crossing (Fig. 5a) indicate that these molecular entities are able to

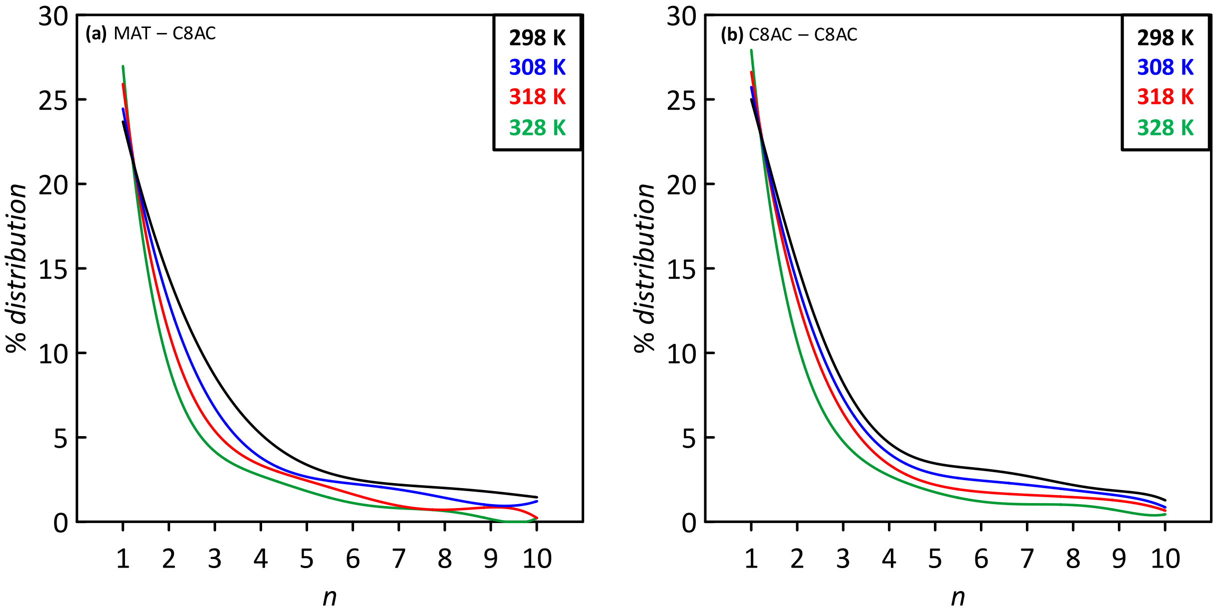

Fig. 11. Percentage distribution of cluster size, *n* (1 stands for monomer, 2 per dimer, etc, for MAT:C8AC (1:1) LMMs as a function of temperature. In panel a, results for MAT–C8AC clusters (per MAT molecule) and in panel b, results for C8AC–C8AC clusters (per C8AC molecule).

efficiently interact with the considered model plasma membrane. The large apolar nature of the MAT:C8AC pairs allows an efficient fitting of the molecular entity into the bilayer. These results justify the reported experimental cytotoxicity (measured with CCK-8 assay) [38], which led to $IC_{50} = 0.91$ mg mL^{-1} for MAT;C8AC (1:1), with increasing cytotoxicity for the LMM in comparison with neat MAT, which would be justified considering the increase of hydrophobicity and the properties reported in Figs. 4 and 5. Likewise, these results agree with those in the literature showing strong effects of amphiphilic DES/LMM on eukaryotic cells [62], and therefore it would be the main drawback on the considered LMMs. Nevertheless, two key points should be considered regarding the potential cytotoxicity of the LMM in question: *i*) the reported experimental IC_{50} (2.3 mM) although large, indicates moderate toxicity, and is larger compared to other DES/NADES/LMM [63], and *ii*) the extremely low water solubility (Fig. 4b) would hinder reaching such concentrations, ultimately resulting in higher cell viability, i.e. lower toxicity. Two possible exposure routes may be considered for toxicity effects of the LMM: *i*) inhalation, which must be discarded by the close to null vapor pressure reported in Fig. 4c, and *ii*) contamination of water with LMM during PFOA (PFAS) extraction and thus, toxicity via ingestion of treated drinking water, which much be discarded the low water solubility of the considered LMM, which will hinder water cross-contamination during water treatment. Regarding the biodegradability and persistence in water, QSAR calculations [64] show biodegradable and non-persistant character. Therefore, although the reported results for the effective interaction of the LMM with plasma cell membranes indicate effective penetration and stabilization of the molecules inside the bilayers, the apolar character of the molecules combined with their low concentration would lead to minor disruptions in membranes properties, i.e. negligible toxicity. Similarly, the low water solubility as well as negligible vapor pressure would lead to negligible human exposure via respiratory or digestive routes, and thus, the considered LMM may be considered as safe and sustainable.

3.1.4. Aggregation properties of MAT:C8AC (1:1) LMM

Once the main macroscopic, environmental and toxicological properties of MAT:C8AC are established, the nanoscopic properties of this LMM were studied using MD simulations. The reliability of MD results stands on the suitability of the considered forcefield (COMPASS III) to describe the considered LMM. To check this reliability, selected relevant thermophysical properties (density, ρ, and isobaric thermal expansion coefficient, α_p) as inferred from MD simulations, were compared with those experimental reported in the literature [39], Fig. 6. MD simulations led to slightly lower values for both properties, but the average deviations (1.2 and 4.2 %) as well as the slope of ρ or α_p vs temperature show reliable predictions, thus validating the MD approach.

The MD analysis provided structural information in terms of molecular arrangements and intermolecular interactions. To analyse the possible interacting pairs considering the potential donor–acceptor sites, as inferred from DFT results in Fig. 2, Radial Distribution Functions (RDFs) for all the atomic pairs were calculated and systematically examined and organized using the connection matrix (*cmat*) function. The *cmat* combines in a plot (contact matrix) the first peak's height and distance for the RDFs of interacting pairs, Fig. 7. The *cmat* results indicate two main features: *i*) MAT–C8AC interaction via MAT(O1) and MAT (N2) acceptor sites, corresponding to hydrogen bonding with the C8AC (OH) donor site, discards relevant interaction with MAT(N1), in agreement with DFT results for the strength of hydrogen bonding, and *ii*) C8AC self-association via hydrogen bonding among O1 (OH donor) and O2 (acceptor) sites. These features, suffer minor changes within the temperature range 298–328 K studied. Relevant RDFs are reported in Fig. 8. In the case of MAT–C8AC interaction via the MAT(O1) acceptor site, Fig. 8a, the reported RDFs show a strong and narrow peak, indicating hydrogen bonding, with donor–acceptor distances in agreement with those obtained from DFT results for dimers (Fig. 2a). A slight weakening upon heating can be observed, thus confirming hydrogen bonding (i.e. LMM formation) in the whole temperature range. Additionally, results in Fig. 8b and c confirm C8AC self-association via hydrogen bonding among OH and CO sites, discarding OH–OH interactions. Further details on the nanoscopic arrangements may be inferred from the Spatial Distribution Functions (SDFs) around MAT and C8AC molecules, Fig. 9. In the case of a central MAT molecule, it is clear that C8AC molecules are preferentially placed around the MAT(O1) acceptor site, with lower concentration around the MAT nitrogen sites. However, the concentration around the nitrogen sites increases upon heating. This could be because the additional thermal energy helps overcome steric hindrance barriers, increasing C8AC delocalization around the MAT acceptor sites. In the case of central C8AC molecules, results indicate MAT(O1) concentration around the acid hydroxyl group and hydrogen bonding among neighbor C8AC molecules via the

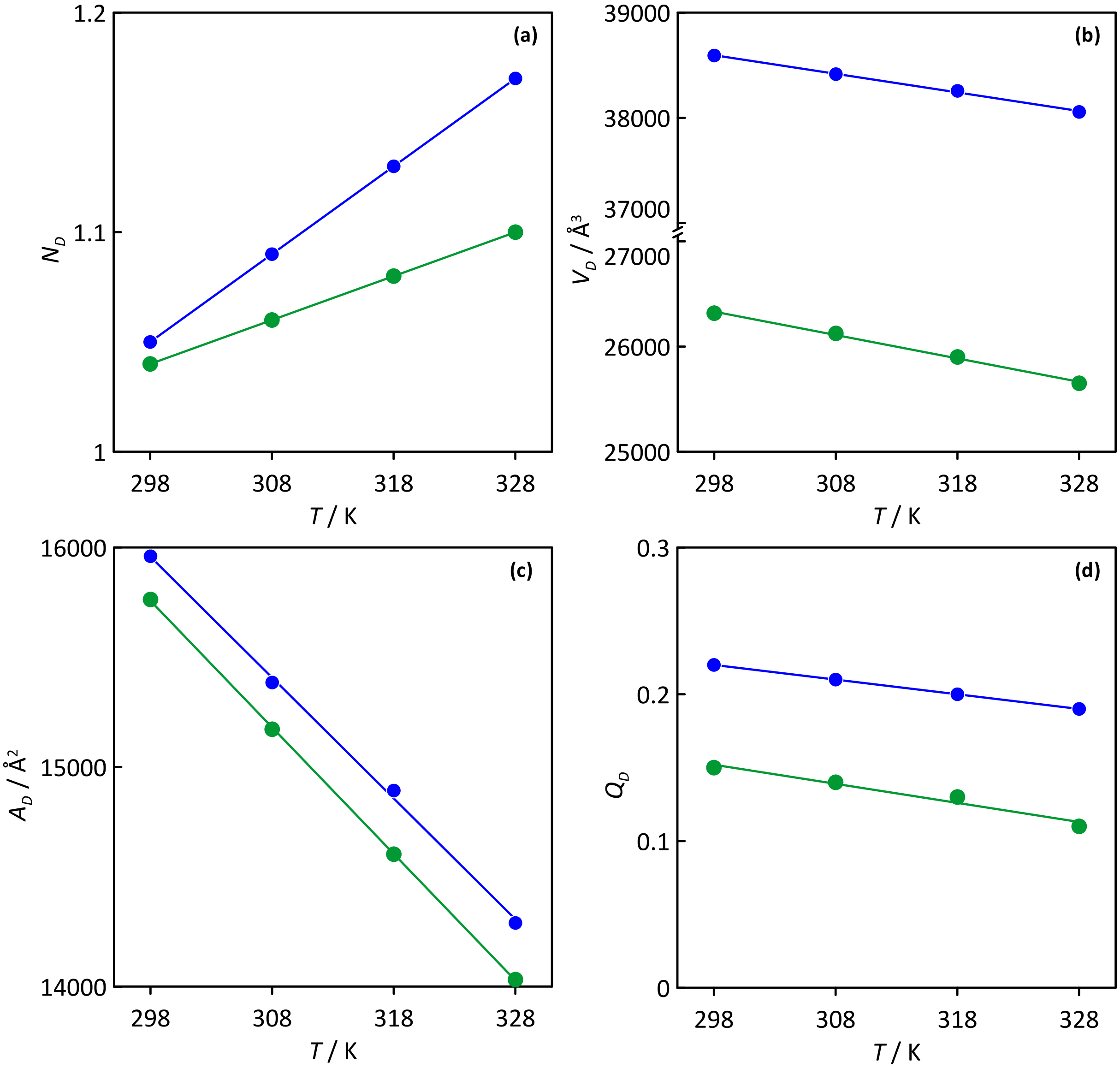

Fig. 12. Domain analysis for MAT and C8AC in MAT:C8AC (1:1) LMMs as a function of temperature. Number of domains, N_D , domain volume, V_D , domain area, A_D, and isoperimetric index of domains, Q_D. (blue) MAT and (green) C8AC.

hydroxyl group.

The topological characteristics of the developed hydrogen bonds are analyzed via the Combined Distribution Functions (CDFs), considering orientation (donor–acceptor angle) and separation (donor–acceptor distance), Fig. 10. In the case of MAT(O1)–C8AC(OH) interaction, the hydrogen bonding leading to the LMM formation, CDF results show a strong spot at 2.7 Å and 175° confirming the formation of a strong largely lineal hydrogen bond, in agreement with DFT results for isolated dimers (Fig. 2), and thus probing how this feature stands on the formation and properties of the considered LMM. Although the reported results depict the formation of MAT–C8AC dimmers via hydrogen bonding, the formation of larger aggregates is also analyzed considering that DFT results in Fig. 2 showed the possibility of molecular aggregation via van der Waals interactions combined with hydrogen bonding. Consequently, a cluster analysis was carried out, Fig. 11. Results for MAT–C8AC clustering, Fig. 11a, indicate prevailing population of small clusters (50 % of total clusters correspond to monomer + dimers + trimmers), but non-negligible larger aggregations are also observed. A similar behavior is inferred for C8AC–C8AC clustering, Fig. 11b. For both types of clusters, the population of monomers is roughly 25 %, thus most of the molecules are involved in hydrogen bonding, with minor increase upon heating up to 328 K, thus confirming the large trend to hetero (MAT–C8AC) and homo (C8AC–C8AC) associations in the liquid phase. Further analysis of liquid structuring is carried out through the domain analysis for MAT and C8AC molecules (Fig. 12). The calculated number of domains (Fig. 12a) indicate values close to unit for both molecules and slightly increasing with temperature, which corresponds to connected domains along the fluid structure, i.e. all molecules are interconnected in domains via de developed hydrogen bonds and van der Waals interactions. The developed domains have large volume (larger for MAT than for C8AC) and surfaces, Fig. 12b and c, that diminish with temperature, and are non-spherical, as inferred form the low isoperimetric index (Fig. 12d).

3.1.5. Interaction dynamics of MAT:C8AC (1:1) LMM

The dynamic behavior of the LMM is also analyzed from MD results starting from those for the developed hydrogen bonds. The DFT results indicated strong hydrogen bonds which were also confirmed by MD in the considered liquid phases. The dynamic properties of these interactions were analyzed considering two key aspects: the lifetime once

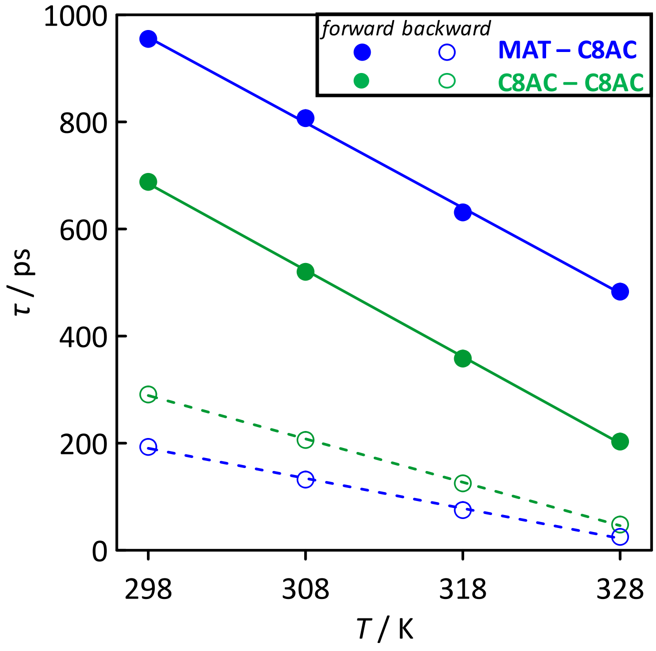

Fig. 13. Dynamic properties of the reported hydrogen bonds showing the times, τ, for forward (hydrogen bond lifetime) and backward (hydrogen bond time for reforming after breaking) processes, for MAT:C8AC (1:1) LMMs as a function of temperature.

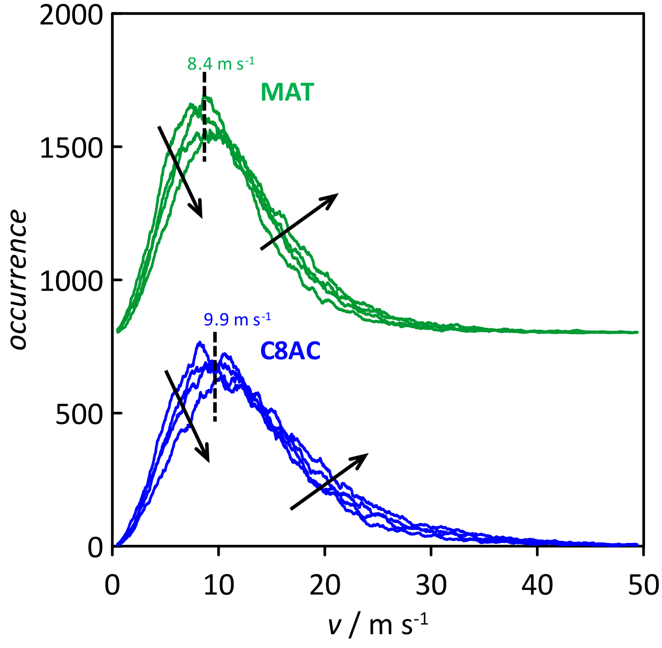

Fig. 14. Center-of-mass velocity distribution functions, v, for MAT and C8AC in MAT:C8AC (1:1) LMMs as a function of temperature. Values indicate the average v value for the maxima in the studied temperature range. Arrows indicate increasing temperature from 298 to 328 K in 10 K steps.

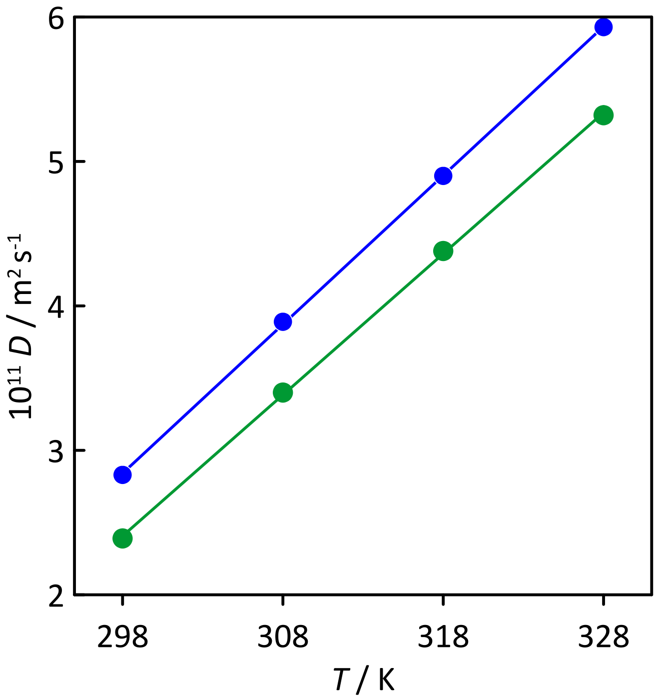

Fig. 15. Center-of-mass self-diffusion coefficient, D, for MAT and C8AC in MAT:C8AC (1:1) LMMs as a function of temperature.

an hydrogen bond is formed (forward dynamic process) and the required time for the formation of a new hydrogen bond (reforming time) once a site is available after hydrogen bonding breaking (backward dynamic process), Fig. 13. The lifetimes of MAT–C8AC are larger than those for C8AC–C8AC ones and decrease upon heating. The lifetime of MAT–C8AC hydrogen bonds (e.g. 0.96 ns at 298 K) is lower than those of most DES reported in the literature, e.g. a literature analysis of 38 known DES showed a 2.67 ns average lifetime for the corresponding HBA–HBD hydrogen bonding [65]. This figure suggests a more dynamic picture for MAT–C8AC interaction in spite of the strength of this hydrogen bonding (Fig. 2). This more dynamic character is confirmed by the low reforming times (e.g. 0.2 ns for MAT–C8AC at 298 K), i.e., a very dynamic picture of the hydrogen bonding formation and reforming is inferred both for MAT–C8AC and C8AC–C8AC interactions.

The dynamics of the LMM was firstly analyzed considering the center-of-mass velocity distribution functions (VDFs) for MAT and C8AC, reported in Fig. 14. The first relevant RDF result anticipate the pairing of MAT and C8AC VDFs, with maxima around 9–10 m/s for both molecules, which corresponds to paired diffusion in agreement with the developed MAT–C8AC hydrogen bonding. Likewise, the low velocities correspond to the viscous character of the LMM (391.4 mPa s at 298.15 K [39]). The paired MAT–C8AC diffusion is confirmed by the center-of-mass self-diffusion coefficients, Fig. 15, showing slow diffusion rates for both compounds and parallel evolution with temperature.

3.2. Extractive ability of MAT:C8AC (1:1) LMM for PFOA from water

Once the proposed LMM was analysed, its behavior with regard to PFOA was studied. As the LMM should efficiently extract the PFOA, a large LMM–PFOA affinity is expected. This interactiong is studied via DFT, considering MAT–C8AC–PFOA (1:1: 1) trimmers, taking into account a total of 10 possible LMM–PFOA interacting sites (as inferred from the exploration of the molecular interacting sites), Fig. 16. The first relevant result is the large LMM affinity for PFOA molecule, with interaction energies in the range of −57 to −155 kJ/mol. Therefore, the considered LMM have two pivotal properties to be used for PFOA removal from polluted waters: *i*) very large affinity for the target molecule and *ii*) negligible solubility in the water phase. The largest LMM–PFOA interaction energies are obtained when PFOA develops hydrogen bonds with MAT (model #01) or with C8AC (models #03, #05, #08 and #10). This versatility of the LMM to develop strong interactions with the PFOA is accompanied with minor disruptions of MAT–C8AC hydrogen bonds, i.e. maintaining the intrinsic LMM integrity from the hydrogen bonding viewpoint. This can be stated in view of

	#01	#02	#03	#04	#05	#06	#07	#08	#09	#10
ΔE / kJ mol^{-1}	-155.4	-66.9	-152.5	-56.7	-57.4	-139.4	-63.3	-144.2	-85.2	-148.9
RMSD	0.39	0.58	1.64	0.56	0.76	1.09	0.62	0.86	0.53	0.00

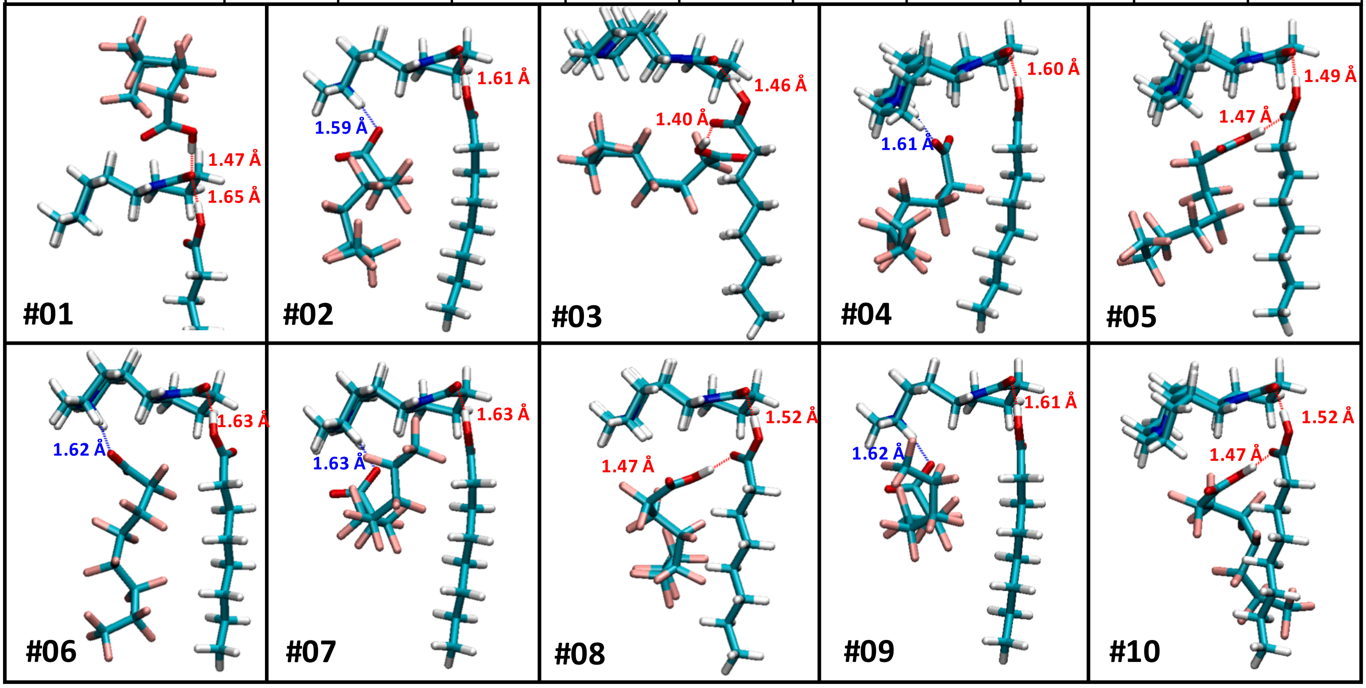

Fig. 16. DFT optimized structures of MAT:C8AC:PFOA (1:1:1) clusters considering different molecular orientations. Relevant hydrogen bonding distances are reported inside each panel for MAT–C8AC and PFOA–MAT/C8AC hydrogen bonds. Likewise, PFOA–LMM interaction energy, Δ*E*, is reported as well as Root Mean Square Deviation for MAT:C8AC(excluding PFOA molecule) wrt #10 cluster.

the corresponding hydrogen bonding distance when interacting with PFOA in comparison with clean dimers, Figs. 2 and 16. The 10 considered interacting clusters leads to minor variations in the structure of the core MAT–C8AC pair, as reported by the small RMSD values, Fig. 16. Therefore, the considered LMM have a large versatility to develop proper and strong interactions with PFOA molecules.

As the final purpose of the LMM is to extract PFAS (PFOA) from a water polluted liquid phase, MD simulations conducted on the biphasic system consisting of a LMM + water and a PFOA solution were carried out, scheme of the simulation box reported in Fig. 17. The first highly promising results stand on the fact that just after 5 ns of MD simulations, all the PFOA molecules (corresponding to 5 wt% content in aqueous phase) have penetrated into the LMM phase leaving the water phase clean. This result, a consequence of the large LMM–PFOA affinity reported in Fig. 16, shows the suitability of the considered LMM to extract PFAS (PFOA) from polluted water phases, Fig. 17. The reported density profiles in the direction perpendicular to the surface shows how initially the PFOA molecules tend to remain in the vicinity of the LMM–water interface, but inside the LMM liquid phase. This behavior result from the development of intermolecular interactions with the accumulated MAT/C8AC molecules in these regions, thus being the root of the initial step of quick PFOA capturing. Results in Fig. 2 (DFT), 9 (MD) and 17 (MD) confirm the extraction mechanism of PFOA as a result of the strong interaction between PFOA and the hydrogen bonding available sites in the considered LMM, without disruption of the interaction with LMM components. This leads to a largely localized interaction for PFOA molecules around LMM molecular sites, keeping the hydrophobic character of the LMM, and thus, extracting the PFOA molecules from waste water without water contamination of the considered LMM extractant.

The interaction of the LMM with the PFOA–aqueous phase, the formation of the interface and the absorption of PFOA could lead to changes in the complex structure of the LMM liquid phase. The calculated RDF for MAT–C8AC main interaction in presence of the interface is reported in Fig. 18a. The hydrogen bonding between MAT (O1) and C8AC(O1), which as probed in Section 3.1, that was on the root of the LMM formation, is preserved and even reinforced for those LMM molecules in the interface. The only different feature for molecules at the interface is the vanishing of the second (wide) peak, which results from the confinement effect of those molecules in the interface region allowing only more oriented interactions. This effect is confirmed by the results reported in Fig. 18b, which show how both MAT and C18AC molecules at the interface region develop preferential perpendicular orientations to the interface, but maintaining their intermolecular hydrogen bonding (Fig. 18a).

Likewise, the application of COSMOtherm for the prediction of PFOA solubility in the considered LMM indicates a value of 0.67 g g^{-1} at 298.15 K (the predicted solubility in water being 9.6 • 10^{-4} g g^{-1}, i.e. PFOA is 906 times more soluble in the considered LMM than in water). This result confirms the suitability of this solvent for the extraction of PFOA from aqueous phases, both from thermodynamic and kinetic (Fig. 17) viewpoints. The large solubility of PFOA in the LMM assures the reusability of the considered LMM as extractant from pollute waters. The usual concentration of PFAS in polluted and drinking waters use to be in the ng/L range [66], which allows reusability through continuous cycles without loss of efficiency [67], and thus decreasing water treatment costs.

3.3. *Searching of PFOA extraction improvement around MAT molecular moiety*

Once the suitability of MAT:C8AC (1:1) LMM for PFAS (PFOA) extraction has been proved, this system was used as starting point for the development of even better PFOA extractive solvents. This development considers a holistic view of all the relevant physicochemical, technological, environmental and safety related properties. First, a collection of

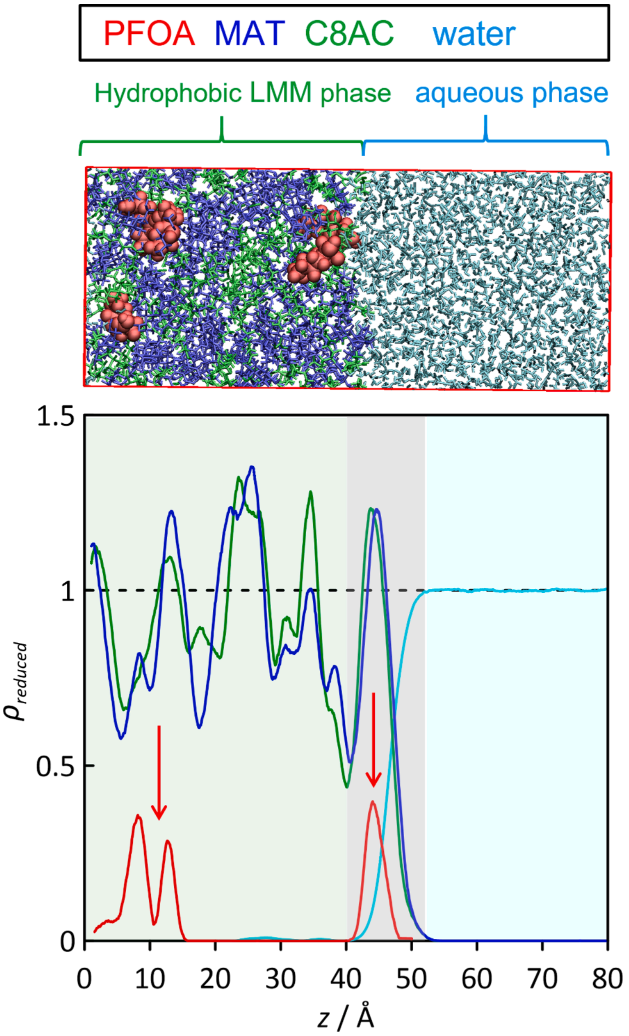

Fig. 17. Snapshot after 5 ns of MD simulation showing the structure of MAT:C8AC (1:1) + water interface at 308 K and 1 bar. Center-of-mass reduced density, $\rho_{reduced}$ (calculated with reference to the corresponding densities in the bulk liquid phases) in the direction perpendicular to the interface is reported. Gray shaded area shows the interface as defined with reference to aqueous phase (interface width = 1.2 Å).

101 molecules were extracted from the Zinc molecular Database [53], considering their similarity with MAT molecules, using Tanimoto similarity index as selection criterion, Fig. 19a. The possible formation of LMM among those MAT-related compounds and fatty acids with chain length in the C6 to C12 range was analyzed by the prediction of the eutectic point and composition, Fig. 19b and 19c. The reported results show a large collection of hypothetical LMM with eutectic melting temperatures below ambient temperature, i.e. liquid at ambient conditions and thus suitable to be used as liquid extracting solvents. Likewise, PFOA solubility was predicted in all those LMM being liquid at ambient conditions, Fig. 19d.

To find the most suitable combination, a collection of descriptors were predicted: *i*) environmentally relevant properties (Supplementary Information): octanol–water partition coefficient (the larger, the better) to avoid aqueous phase cross-contamination and vapor pressure (the lower, the better) to avoid atmospheric contamination, *ii*) safety related properties: toxicity indicators (the smaller, the better), *iii*) synthetic accessibility score (the lower the better), and *iv*) PFOA solubility in solvent mass base. All this information was combined in a single score (0–1 range, the larger, the better), Fig. 20, and the most suitable combination (higher score) was selected. The elected LMM result in a MAT modification including an hydroxyl group combined with C8AC fatty acid. This modification results in an improvement of PFOA solubility, from 0.67 g g^{-1} for MAT–C8AC to 0.90 g g^{-1} for the new LMM, decreasing toxicity (lower log($IGC50^{-1}$)), for a compound with 4.18 synthetic accessibility score. Therefore, the developed LMM (Fig. 20) can be considered as a further improvement of MAT–fatty acid LMM for PFAS (PFOA) extraction from polluted water according to the principles of Safe, Sustainable and Functional by Design solvent.

4. Conclusions

This study comprehensively investigated the properties and performance of a novel hydrophobic natural Low Melting Mixture composed of matrine and caprylic acid for the extraction of perfluorooctanoic acid (PFOA) as an archetype and abundant PFAS from polluted water. Through a multi-faceted computational approach combining quantum DFT calculations, molecular dynamics simulations (MD), and COSMO-therm predictions, the efficacy, environmental sustainability, safety and scalability of this solvent for PFOA removal was investigated. The main findings may be summarized as follows:

- *i*) The MAT:C8AC (1:1) LMM exhibits strong hydrogen bonding, leading to a stable and highly hydrophobic solvent with negligible water solubility and vapor pressure.
- *ii*) Despite its ability to interact with lipid bilayers, the LMM shows relatively low cytotoxicity due to its extremely low water solubility.
- *iii*) The LMM demonstrates excellent PFOA extraction capabilities, from thermodynamics and kinetics viewpoints, with PFOA being 906 times more soluble in the LMM than in water.
- *iv*) A modified developed version of the LMM, incorporating a hydroxyl group in the MAT molecule, further improves PFOA solubility while maintaining low toxicity.

These results highlight the potential of LMM as an environmentally friendly and efficient alternative for PFAS removal from contaminated water sources. Future research should focus on scaling up the process, investigating the extraction of other PFAS compounds, and exploring the recyclability of the LMM for sustainable long-term use in water treatment applications.

CRediT authorship contribution statement

Sonia Martel-Martlin: Writing – review & editing, Writing – original draft, Supervision, Project administration, Investigation, Formal analysis, Data curation, Conceptualization. **Nuria Aguilar:** Writing – review & editing, Writing – original draft, Visualization, Validation, Investigation, Formal analysis, Data curation, Conceptualization. **Alberto Gutiérrez:** Writing – review & editing, Writing – original draft, Validation, Supervision, Methodology, Investigation, Formal analysis, Data curation, Conceptualization. **Sara Rozas:** Writing – review & editing, Writing – original draft, Visualization, Validation, Supervision, Investigation, Formal analysis, Data curation, Conceptualization. **Pedro A. Marcos:** Writing – review & editing, Writing – original draft, Validation, Supervision, Methodology, Investigation, Formal analysis, Data curation, Conceptualization. **Alfredo Bol:** Writing – review & editing, Writing – original draft, Validation, Supervision, Investigation, Formal analysis, Data curation, Conceptualization. **Mert Atilhan:** Writing – review & editing, Writing – original draft, Validation, Supervision, Investigation, Data curation, Conceptualization. **Jose L. Trenzado:** Writing – review & editing, Writing – original draft, Validation, Supervision, Methodology, Investigation, Data curation, Conceptualization. **Santiago Aparicio:** Writing – review & editing, Writing – original draft, Visualization, Validation, Supervision, Software, Resources, Project administration, Methodology, Investigation, Funding acquisition, Data curation, Conceptualization.

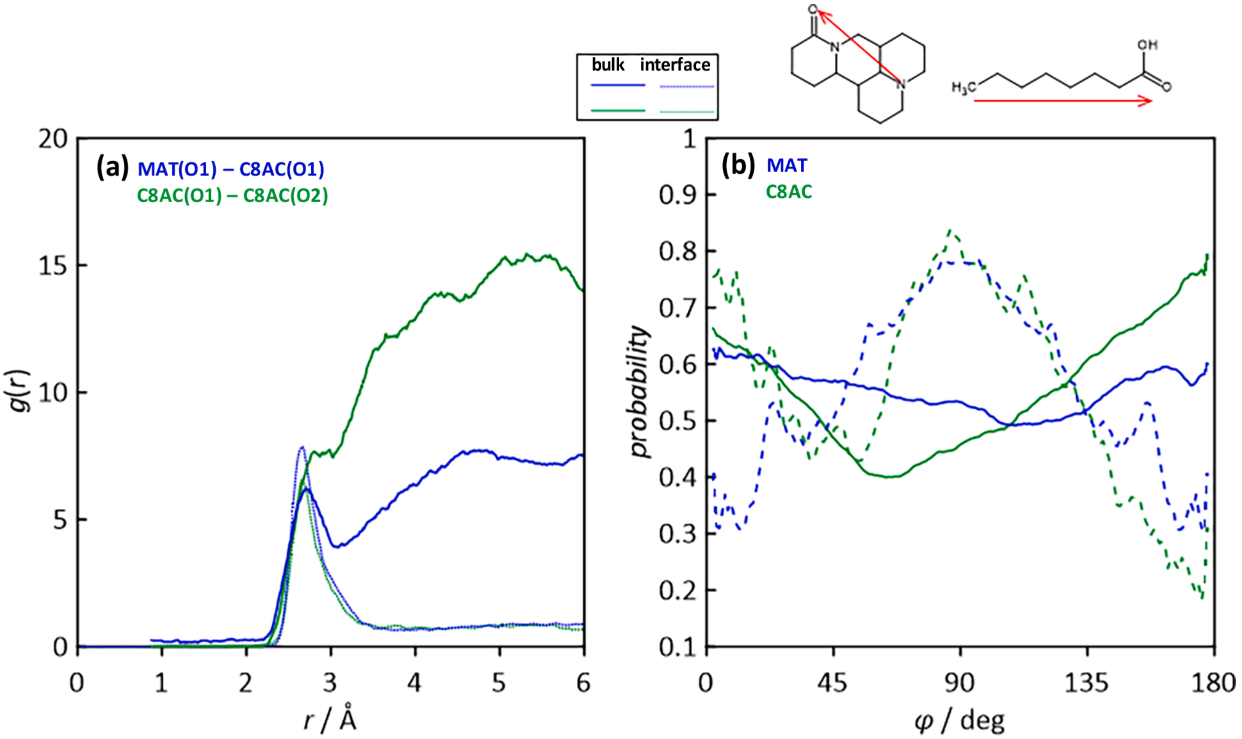

Fig. 18. Comparison for the reported properties among the bulk liquid phase (in absence of interface) and MAT:C8AC (1:1) + water interface after extraction of PFOA molecules from aqueous phase at 308 K and 1 bar. Panel a shows Radial Distribution Functions (atom labelling as in Fig. 1) for the reported pairs and panel b shows distribution for the angle (φ) formed the reported molecular vectors (red arrows) and the z-vector (perpendicular to the interface).

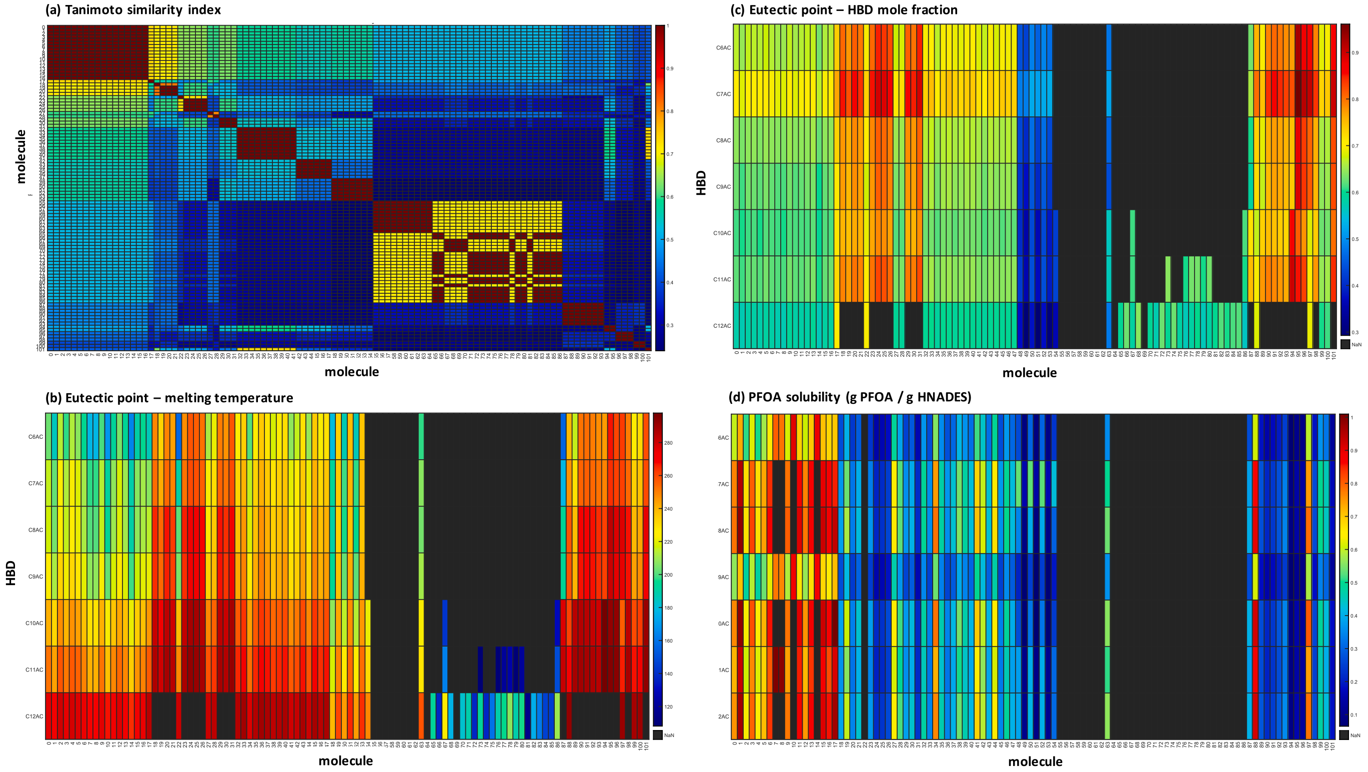

Fig. 19. Heat maps for relevant properties related with molecules designed from MAT (MAT-derived molecules). (a) Tanimoto similarity index among molecules; properties for the eutectic point in the Solid–Liquid equilibria for the LMM formed by MAT-derived molecules and fatty acids as HBDs showing (b) eutectic temperature and (c) fatty acid mole fraction for the eutectic point; (d) PFOA solubility at 298.15 K in the LMM formed by combination of MAT-derived molecules:fatty acids (1:1 ratio). Results in panels b to d obtained from COSMOtherm calculations.

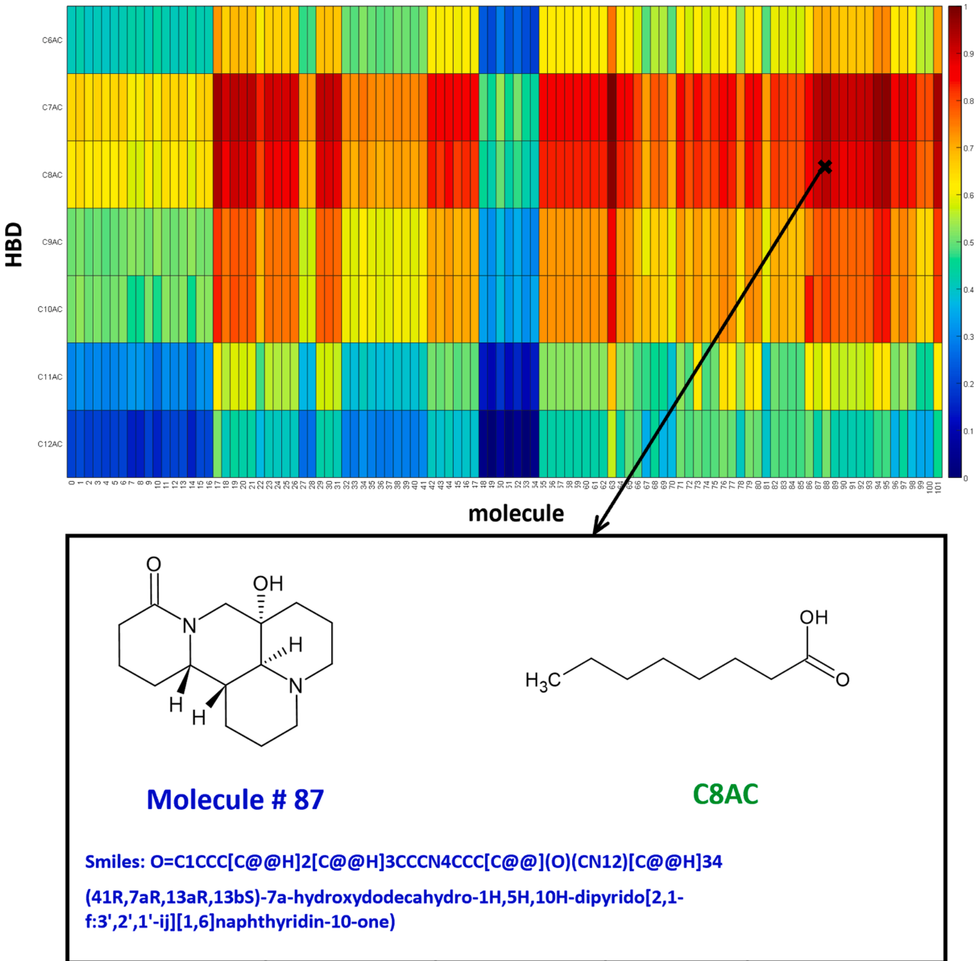

Smiles: O=C1CCC[C@@H]2[C@@H]3CCCN4CCC[C@@](O)(CN12)[C@@H]34

(41R,7aR,13aR,13bS)-7a-hydroxydodecahydro-1H,5H,10H-dipyrido[2,1-f:3',2',1'-ij][1,6]naphthyridin-10-one)

PFOA solubility (at 298.15 K) / g g^{-1}	T_m / K	solubility in water (at 298.15 K) / g g^{-1}	P_{vap} (at 298.15 K) / Pa	log(IGC50^{-1})
0.90	257.5	0.02	0.00003	-1.17

Fig. 20. Results of scoring for molecules designed from MAT showing the selected new LMM with relevant properties.

Declaration of competing interest

The authors declare that they have no known competing financial interests or personal relationships that could have appeared to influence the work reported in this paper.

Acknowledgements

This work was funded by European Union (Horizon 2020 program, project WORLD: H2020-MSCA-RISE-2019-WORLD-GA-873005), and Agencia Estatal de Investigación (Project NADESforPFAS: PID2022-142405OB-I00). Author Alberto Gutiérrez received grant BG22/00089 funded by Spanish Ministerio de Universidades. We also acknowledge SCAYLE (Supercomputación Castilla y León, Spain) for providing supercomputing facilities. The statements made herein are solely the responsibility of the authors.

Appendix A. Supplementary material

Screening_results.xlsx (molecules designed from MAT as possible DES formers with fatty acids). Supplementary data to this article can be found online at https://doi.org/10.1016/j.molliq.2025.127142.

Data availability

Data will be made available on request.

References

[1] L.G.T. Gaines, Historical and current usage of per- and polyfluoroalkyl substances (PFAS): a literature review, Am. J. Ind. Med. 66 (2023) 353–378.

[2] J. Glüge, M. Scheringer, I.T. Cousin, J.C. DeWitt, G. Goldenman, D. Herzke, R. Lohmann, C.A. Ng, X. Trier, Z. Wang, An overview of the uses of per- and polyfluoroalkyl substances (PFAS), Environ. Sci. Processes Impacts 22 (2020) 2345–2373.

[3] Z. Zhang, D. Sarkar, J.K. Biswas, R. Datta, Biodegradation of per- and polyfluoroalkyl substances (PFAS): a review, Biores. Technol. 344 (2022) 126223.

[4] B. Xu, S. Liu, J.L. Zhou, C. Zheng, W. Jin, B. Chen, T. Zhang, W. Qiu, PFAS and their substitutes in groundwater: occurrence, transformation and remediation, J. Hazard. Mater. 412 (2021) 125159.

[5] Regulation (EU) 2019/1021 of the European Parliament and of the Council of 20 June 2019 on Persistent Organic Pollutants, https://eur-lex.europa.eu/legal-content/en/TXT/PDF/?uri=CELEX:02019R1021-20230828&from=EN.

[6] H.N.P. Vo, H.H. Ngo, W. Guo, T.M.H. NguyeN, J. Li, H. Liang, L. Deng, Z. Chen, T. A.H. Nguyen, Poly-and perfluoroalkyl substances in water and wastewater: a comprehensive review from sources to remediation, J. Water Proc. Eng. 36 (2020) 101393.

[7] G.M. Sinclair, S.M. Lang, O.A.H. Jones, What are the effects of PFAS exposure at environmentally relevant concentrations? Chemosphere 258 (2020) 127340.

[8] A.V. Shirke, E.G. Radke, C. Lin, R. Blain, N. Vetter, C. Lemeris, P. Hartman, H. Hubbard, M. Angrish, X. Arzuaga, J. Congleton, A. Davis, L.V. Dishaw, R. Jones, R. Hudson, P. Kaiser, A. Kraft, L. Lizarragam, P.D. Noyes, G. Patlewicz, M. Taylor, A.J. Williams, K.A. Thayer, L.M. Carlson, Environ. Health Pers. 132 (2024) 026001.

[9] M. Sadia, I. Nollen, R. Helmus, T.L. ter Laak, F. Been, A. Praetorius, A.P. Van Wezel, Occurrence, fate, and related health risks of PFAS in raw and produced drinking water, Environ. Sci. Technol. 57 (2023) 3062–3074.

[10] https://www.epa.gov/sdwa/and-polyfluoroalkyl-substances-pfas.

[11] https://echa.europa.eu/substances-restricted-under-reach.

[12] R. Amen, A. Ibrahim, W. Shafqat, E. Hassan, A critical review on PFAS removal from water: removal mechanism and future challenges, Sustainability 15 (2023) 16173.

[13] S. Yadav, I. Ibrar, R.A. Al-Jubaori, L. Singh, N. Ganbat, T. Kazwini, E. Karbassiyazdi, A.K. Samal, S. Subbiah, A. Altaee, Updated review on emerging technologies for PFAS contaminated water treatment, Chem. Eng. Res. Des. 182 (2022) 667–700.

[14] B. Cantoni, A. Turolla, J. Wellmitz, A.S. Ruhl, M. Antonelli, Perfluoroalkyl substances (PFAS) adsorption in drinking water by granular activated carbon: Influence of activated carbon and PFAS characteristics, Sci. Total Environ. 795 (2021) 148821.

[15] N. Belkoputeb, V. Franke, P. McCleaf, S. Köhler, L. Ahrens, Removal of per- and polyfluoroalkyl substances (PFASs) in a full-scale drinking water treatment plant: long-term performance of granular activated carbon (GAC) and influence of flow-rate, Water Res. 182 (2020) 115913.

[16] V. Franke, M. Ullberg, P. McCleaf, M. Wällinder, S.J. Köhler, L. Ahrens, The price of really clean water: combining nanofiltration with granular activated carbon and anion exchange resins for the removal of per- and polyfluoralkyl substances (PFASs) in drinking water production, ACS EST Water 1 (2021) 782–795.

[17] F. Dixit, R. Dutta, B. Barbeau, P. Beruube, M. Mohseni, PFAS removal by ion exchange resins: a review, Chemosphere 272 (2021) 129777.

[18] Y.L. Liu, M. Sun, Ion exchange removal and resin regeneration to treat per- and polyfluoroalkyl ether acids and other emerging PFAS in drinking water, Water Res. 207 (2021) 117781.

[19] S. Zahmatkesh, Z. Chen, N.A. Khan, B.J. Ni, Removing polyfluoroalkyl substances (PFAS) from wastewater with mixed matrix membranes, Sci. Total Environ. 912 (2024) 168881.

[20] M. Chaudhary, M. Sela-Adler, A. Ronen, O. Nir, Efficient PFOA removal from drinking water by a dual-functional mixed-matrix-composite nanofiltration membrane, npj Clean Water 6 (2023) 77.

[21] C. Liu, X. Zhao, A.F. Faria, K.Y.D. Quiñones, C. Zhang, Q. He, Y. Shen, Y. Zhi, Evaluating the efficiency of nanofiltration and reverse osmosis membrane processes for the removal of per- and polyfluoroalkyl substances from water: a critical review, Sep. Purif. Technol. 302 (2022) 122161.

[22] M.N. Taher, S.A. Al-Mutwalli, S. Barisci, D.Y. Kaseoglu-imer, L.F. Dumee, M.M. A. Shirazi, Progress on remediation of per- and polyfluoroalkyl substances (PFAS) from water and wastewater using membrane technologies: a review, J. Water Process Eng. 59 (2024) 104858.

[23] B. Xu, M.B. Ahmed, J. Zhou, A. Altaee, M. Wu, Photocatalytic removal of perfluoroalkyl substances from water and wastewater: mechanism, kinetics and controlling factors, Chemosphere 189 (2017) 717–729.

[24] B. Lashuk, M. Pineda, S. AbuBakr, D. Baffito, V. Yargeau, Application of photocatalytic ozonation with a WO3/TiO2 catalyst for PFAS removal under UVA/visible light, Sci. Total Environ. 843 (2022) 157006.

[25] M. Veciana, J. Brauning, A. Forhat, M.L. Pype, S. Freguia, G. Carvalho, J. Keller, P. Ledezma, Electrochemical oxidation processes for PFAS removal from contaminated water and wastewater: fundamentals, gaps and opportunities towards practical implementation, J. Hazard. Mater. 434 (2022) 128886.

[26] S. Sharma, N.P. Shetti, S. Basu, M.N. Nadagouda, T.M. Aminabhavi, Remediation of per- and polyfluoroalkyls (PFAS) via electrochemical methods, Chem. Eng. J. 430 (2022) 132895.

[27] D.O. Abranches, J.A.P. Coutinho, Everything you wanted to know about deep eutectic solvents but were afraid to be told, Ann. Rev. Chem. Biochem. Eng. 14 (2023) 141–163.

[28] Y. Liu, J.B. Friesen, J.B. McAlpine, D.C. Lankin, S.N. Chen, G.F. Pauli, Natural deep eutectic solvents: properties, applications, and perspectives, J. Nat. Prod. 81 (2018) 679–690.

[29] M. Vieira-Sanches, R. Freitas, M. Oliva, A. Mero, L. De Marchi, A. Cuccaro, G. Fumagalli, A. Mezzetta, G.C. Dugoni, M. Ferro, A. Mele, L. Guazzelli, C. Pretti, Are natural deep eutectic solvents always a sustainable option? A bioassay-based study, Environ. Sci. Poll. Res. 30 (2022) 17268–17279.

[30] J. Zuo, S. Geng, P. Ma, Z. Fan, Y. Zhang, A. Dong, Current progress in natural deep eutectic solvents for the extraction of active components from plants, Crit. Rev. Anal. Chem. 53 (2023) 177–198.

[31] J. Cao, E. Su, Hydrophobic deep eutectic solvents: the new generation of green solvents for diversified and colorful applications in green chemistry, J. Clean. Prod. 314 (2021) 127965.

[32] A. Kyriakoudi, A. Tsiouras, I. Mourtzinos, Extraction of lycopene from tomato using hydrophobic natural deep eutectic solvents based on terpenes and fatty acids, Foods 11 (2022) 2645.

[33] S. Panchabi, J. Beranek, M. Kuentz, Hydrophobic deep eutectic solvent (HDES) as oil phase in lipid-based drug formulations, Int. J. Pharm. 661 (2024) 124418.

[34] M. Marcherl, M.P. Rayaroth, C. Wang, L. Kong, A.A. Khan, G. Baczkaj, Hydrophobic (deep) eutectic solvents (HDESs) as extractants for removal of pollutants from water and wastewater – a review, Chem. Eng. J. 475 (2023) 144971.

[35] L. Fortunato, L.A. Fuhaid, S. Murgolo, C. De Ceglie, G. MascOLO, L. Favlivene, J. S. Vrouwenvelder, G.J. Witkamp, A. Farinha, Removal of polyfluoroalkyl substances (PFAS) from water using hydrophobic natural deep eutectic solvents (NADES): a proof of concept study, J. Wat. Proc. Eng. 56 (2023) 104401.

[36] M.H. Zainal-Abidin, M. Hayyan, W.F. Wong, Hydrophobic deep eutectic solvents: current progress and future directions, J. Ind. Eng. Chem. 97 (2021) 142–162.

[37] J. Wu, T. Xin, Insight into the physicochemical properties and bioactivities of therapeutic deep eutectic solvents based on matrine and fatty acids, J. Mol. Liq. 160 (2022) 119560.

[38] M. Li, J. Yuan, Q. Yang, Z. Liu, S. Meng, X. Wang, C. Peng, T. Yin, Therapeutic deep eutectic solvents based on natural product matrine and caprylic acid: physical properties, cytotoxicity and formation of surfactant free microemulsion, J. Drug Del. Sci. Technol. 90 (2023) 105177.

[39] D.O. Abranches, L.P. Silva, M.A.R. Martins, S.P. Pinho, Understanding the formation of deep eutectic solvents: betaine as a universal hydrogen bond acceptor, ChemSusChem 13 (2020) 4916–4921.

[40] Y. Chen, Z. Yu, Low-melting mixture solvents: extension of deep eutectic solvents and ionic liquids for broadening green solvents and green chemistry, Green Chem. Eng. (2023), https://doi.org/10.1016/j.gce.2023.11.001.

[41] S. Kurwadkar, J. Dane, S.R. Kanel, M.N. Nadagouda, R.W. Cowdrey, B. Ambae, G. C. Struckoff, R. Wilkin, Per- and polyfluoroalkyl substances in water and wastewater: a critical review of their global occurrence and distribution, Sci. Tot. Environ. 809 (2022) 151003.

[42] S. Grimme, J. Antony, H. Krieg, A consistent and accurate ab initio parametrization of density functional dispersion correction (DFT-D) for the 94 elements H-Pu, J. Chem. Phys. 132 (2010) 154104.

[43] S.G. Balasubramani, G.P. Chen, S. Coriani, M. Diedenhofen, M.S. Frank, Y. J. Franzke, F. Furche, R. Grotjahn, M.E. Harding, C. Hättig, A.H.B. Helmich-Paris, et al., J. Chem. Phys. 152 (2020) 184107.

[44] S. Simon, M. Duran, J. Dannenberg, How does basis set superposition error change the potential surfaces for hydrogen-bonded dimers? J. Chem. Phys. 105 (1996) 11024.

[45] R.F.W. Bader, Atoms in molecules, Acc. Chem. Res. 18 (1985) 9–15.

[46] T. Lu, F. Chen, Multiwfn: a multifunctional wavefunction analyzer, J. Comput. Chem. 33 (2012) 580–592.

[47] F. Fuster, B. Silvi, Does the topological approach characterize the hydrogen bond? Theor. Chem. Acc. 104 (2000) 13–21.

[48] E.R. Johnson, S. Keinan, P. Mori-Sanchez, J. Contreras-García, A.J. Cohen, W. Yang, J. Am. Chem. Soc. 132 (2010) 6498–6506.

[49] BIOVIA COSMOtherm, Release 2021; Dassault Systèmes, http://www.3ds.com.

[50] J.A.H. Schwöbel, A. Ebert, K. Bitterman, U. Huniar, K.U. Goss, A. Klamt, COSMOperm: mechanistic prediction of passive membrane permeability for neutral compounds and ions and its pH dependence, J. Phys. Chem. B 124 (2020) 3343–3354.

[51] T.E. Allen, J.M. Goodman, S. Gutsell, P.J. Russell, Defining molecular initiating events in the adverse outcome pathway framework for risk assessment, Chem. Res. Toxicol. 27 (2014) 2100–2112.

[52] T.M. Abdelghany, A.C. Leitch, I. Nevjestic, I. Ibrahim, S. Miwa, C. Wilson, S. Heutz, M.C. Wright, Emerging risk from “environmentally-friendly” solvents: interaction of methylimidazolium ionic liquids with the mitochondrial electron transport chain is a key initiation event in their mammalian toxicity, Food Chem. Technol. 145 (2020) 111593.

[53] N. Aguilar, S. Rozas, E. Escamilla, C. Rumbo, S. Martel, R. Barros, P.A. Marcos, A. Bol, S. Aparicio, Theoretical multiscale study on the properties, aqueous solution behavior and biological impact of zinc oxide nanoparticles, Surf. Interf. 46 (2024) 103965.

[54] J.J. Irwin, K.G. Tang, J. Young, C. Dandarchuluun, B.R. Wong, M. Khurelbaatar, Y. S. Moroz, J. Mayfield, R.A. Sayle, ZINC20—a free ultralarge-scale chemical database for ligand discovery, J. Chem. Inf. Model. 60 (2020) 6065–6073.

[55] I. Sushko, S. Novotarskyi, R. Körner, A.K. Pandey, M. Rupp, W. Teetz, S. Brandmaier, A. Abdelaziz, V.V. Prokopenko, V.Y. Tanchuk, R. Todeschini, A. Varnek, G. Marcou, P. Ertl, V. Potemkin, M. Grishina, J. Gasteiger, C. Schwab, I. L. Baskin, V.A. Palyulin, E.V. Radchenko, W.J. Welsh, V. Kholodovych, D. Chekmarev, A. Cherkasov, J. Aires-de-Sousa, Q.Y. Zhang, A. Bender, F. Nigsch, L. Patiny, A. Williams, V. Tkachenko, I.V. Tetko, Online chemical modeling environment (OCHEM): web platform for data storage, model development and publishing of chemical information, J. Comput. Aided Mol. Des. 25 (2011) 533–554.

[56] RDKit: Open-source cheminformatics, https://www.rdkit.org.

[57] F. Yang, Q. Zheng, H. Tan, X. Wang, Insight into the role of hydrogen bond donor in deep eutectic solvents, J. Mol. Liq. 399 (2024) 124332.

[58] U. Koch, P.L.A. Popelier, Characterization of C-H-O hydrogen bonds on the basis of charge density, J. Phys. Chem. 99 (1995) 9747–9754.

[59] G. Buemi, DFT study of the hydrogen bond strength and IR spectra of formic, oxalic, glyoxylic and pyruvic acids in vacuum, acetone and water solution, J. Phys. Org. Chem. 22 (2009) 933–947.

[60] G. Teizeira, D.O. Abrances, J.A.P. Coutinho, Estimating the melting temperatures of type V deep eutectic solvents, Ind. Eng. Chem. Res. 62 (2023) 14638–14647.

[61] A. Benedetto, Ionic liquids meet lipid bilayers: a state-of-the-art review, Biophys. Rev. 15 (2023) 1909–1939.

[62] F. Cardellini, R. Germani, G. Cardinalli, L. Corte, L. Roscini, N. Spreti, M. Tiecco, Room temperature deep eutectic solvents of (1S)-(+)-10-camphorsulfonic acid and sulfobetaines: hydrogen bond-based mixtures with low ionicity and structure-dependent toxicity, RSC Adv. 5 (2015) 31772–31786.

[63] I.P.E. Macario, H. Oliveira, A.C. Menezes, S.P.M. Vnetura, J.L. Pereira, A.M. M. Goncalves, J.A.P. Coutinho, F.J.M. Goncalves, Cytotoxicity profiling of deep eutectic solvents to human skin cells, Sci. Rep. 9 (2019) 3932.

[64] E. Benfenati, A. Mangerano, G. Gini, VEGA – QSAR: AI inside a platform for predictive toxicology, in: Proceedings of the workshop “Popularize Artificial Intelligence 2013” CEUR Workshop Proceedings, vol. 1107.

[65] U.L. Abbas, Y. Zhang, J. Tapia, S. Md, J. Chen, J. Shi, Q. Shao, Machine-learning-assisted design of deep eutectic solvents based on uncovered hydrogen bond patterns, Engineering (2024), https://doi.org/10.1016/j.eng.2023.10.020.

[66] M. Sadia, I. Nollen, R. Helmus, T.L. ter Laak, F. Been, A. Praetorius, A.P. vaN Wezel, Occurrence, fate, and related health risks of PFAS in raw and produced drinking water, Environ. Sci. Technol. 67 (2023) 3062–3074.

[67] S. Eid, T. Lemanoui, A.S. Darwish, M.A. Jaoude, F. Banat, S.W. Hasan, I.N. AlNahef, Rapid and highly efficient removal of aqueous perfluorooctanoic acid using deep eutectic solvents for sustainable water remediation: an integrated experimental-modeling approach, Chem. Eng. J. 495 (2024) 153668.